Propofol upregulates MFG-E8 in BV2 cells to inhibit pyroptosis mediated by the NF-κB/NLRP3 pathway, thereby ameliorating ischemic-reperfusion neuronal injury

SHEWEI GUO[1], YINGWEI ZHEN[1], GUOSHENG ZHOU[1] and ZHIHUA ZHAO[2]

[1]Department of Neurosurgery, The First Affiliated Hospital of Zhengzhou University, Zhengzhou, Henan 453001, P.R. China;
[2]Department of Neurology, The First Affiliated Hospital of Zhengzhou University, Zhengzhou, Henan 453001, P.R. China

Received November 4, 2025; Accepted February 4, 2026

DOI: 10.3892/ijmm.2026.5786

Abstract. Abnormal activation and pyroptosis of microglia caused by cerebral ischemia-reperfusion injury (CIRI) are key mechanisms underlying neuronal damage. The NF-κB/NLRP3 pathway is a core mediator of microglial pyroptosis and neuroinflammatory cascades in CIRI. Milk fat globule-EGF factor 8 (MFG-E8) is a critical anti-inflammatory and neuroprotective factor. Propofol (PPF) exhibits antioxidant activity and ameliorates neuronal injury, but its effects on CIRI and underlying mechanisms remain unclear. The present study aimed to investigate whether PPF alleviates neuronal injury by modulating NF-κB/NLRP3 pathway via regulating MFG-E8 expression. An oxygen-glucose deprivation/reoxygenation (OGD/R) model was established using mouse microglial BV-2 and hippocampal neuronal HT22 cells and cell survival was assessed via Cell Counting Kit-8 assay. Polarity in BV-2 cells was evaluated using flow cytometry, while cell death was assessed by Calcein AM/PI and TUNEL staining. A transient middle cerebral artery occlusion (tMCAO) mouse model was established and neurological deficit scores were assessed. The impacts of PPF on cortical damage, neuroinflammation, apoptosis and pyroptosis in tMCAO mice were observed by histopathological staining. Inflammatory factor levels were assessed using ELISA kits. Western blotting was performed to assess MFG-E8, pyroptosis and NF-κB/NLRP3 pathway-related proteins. OGD/R decreased viability, increased apoptosis and pyroptosis rates in BV-2 and HT22 cells and promoted M1 polarization in BV-2 cells; PPF treatment reversed these effects. MFG-E8 was downregulated in OGD/R-treated BV2 cells, while PPF upregulated MFG-E8 expression. Additionally, PPF decreased cerebral infarction volume in tMCAO mice, improved neurological deficit score, mitigated pathological brain tissue damage and decreased the number of degenerating neurons. PPF also inhibited pro-inflammatory microglia activation and decreased pro-inflammatory factor levels. Mechanistically, PPF suppressed NF-κB pathway activation and downregulated NLRP3 by upregulating MFG-E8; silencing MFG-E8 reduced the protective effects of PPF in tMCAO mice and OGD/R cell models. PPF improved neuronal injury in CIRI by upregulating MFG-E8 to inhibit pyroptosis induced by the NF-κB/NLRP3 pathway.

Correspondence to: Professor Shewei Guo, Department of Neurosurgery, The First Affiliated Hospital of Zhengzhou University, 1 Jianshe East Road, Erqi, Zhengzhou, Henan 453001, P.R. China
E-mail: gswfeicui@163.com

Key words: propofol, milk fat globule-EGF factor 8, cerebral ischemia reperfusion, NF-κB/NLRP3 pathway, pyroptosis

Introduction

Stroke remains the second primary cause of global death (~7.3 million/year), with ~85% of stroke cases being ischemic strokes (IS) (1-3). IS is a clinical disease due to a cerebral artery or its branch occlusion causing impaired regional cerebral blood supply, leading to localized cerebral tissue ischemia and hypoxic necrosis, which results in neurological deficits (4,5). Cerebral ischemia-reperfusion injury (CIRI) poses a notable challenge in IS management and severely impacts patient outcomes (6). When cerebral blood vessels become blocked, localized brain tissue experiences ischemia and hypoxia. When blood flow is restored, it triggers a series of complex pathological mechanisms (7). Neuroinflammation serves as the key driver of the CIRI pathological process. Under hypoxic-ischemic conditions, microglia undergo rapid activation, releasing large quantities of pro-inflammatory cytokines including tumor necrosis factor-α (TNF-α) and IL-1β, thereby intensifying the inflammatory cascade (8,9). Pyroptosis serves a pivotal role in CIRI-mediated neuronal injury. It further damages the neural microenvironment, exacerbating neuronal death and neurological dysfunction (10,11). Therefore, inhibiting neuronal pyroptosis to decrease neuroinflammation may be an effective approach to enhance the prognosis of CIRI.

Propofol (PPF) is a γ-aminobutyric acid receptor agonist that produces sedative and hypnotic effects by inhibiting neuronal excitability. Its structure contains a phenolic hydroxyl group, thereby conferring antioxidant activity (12,13). In recent years, its research in neuroprotection has garnered notable

attention (12,14). One study indicated that PPF not only alleviates inflammatory responses in microglia but also provides neuroprotection by improving mitochondrial respiratory chain function and glycolytic status (14). Additionally, PPF downregulates the expression of proinflammatory genes induced by lipopolysaccharide (LPS), suppresses neuroinflammatory responses and inhibits excessive activation of microglia (15). In a traumatic brain injury mouse model, Wang *et al* (16) found that PPF downregulates gasdermin (GSDM)D-N and caspase-1 expression, thus inhibiting neuronal pyroptosis. PPF treatment decreases cerebral infarction volume in CIRI mice, decreases the extent of cortical tissue damage and improves neurological function scores (17). Overall, the neuroprotective effects of PPF may involve multiple pathways, including its antioxidant activity, decreased inflammatory responses and inhibition of pyroptosis. However, the specific molecular mechanisms remain unclear.

As a multifunctional glycoprotein, milk fat globule-epidermal growth factor 8 (MFG-E8) enhances phagocytic function and increases the clearance rate of apoptotic cells, thereby alleviating inflammatory responses (18,19). Changes in MFG-E8 expression in the nervous system are associated with neuroprotection and injury repair (20). The NF-κB p/NOD-like receptor protein 3 (NLRP3) pathway is a key signaling pathway mediating neuroinflammatory responses in CIRI (21,22). NF-κB regulates expression of numerous inflammation-related genes, including classic proinflammatory cytokines (IL-1β, IL-6, TNF-α). NLRP3 inflammasome activation promotes the maturation and secretion of proinflammatory cytokines, thus generating a strong inflammatory response (23-25). Excessive activation of the NF-κB/NLRP3 pathway in rat models of intracerebral hemorrhage leads to microglia M1 polarization and induces pyroptosis, thus aggravating neuroinflammation (26). Notably, PPF regulates MFG-E8 expression in microglia (27) and MFG-E8 can downregulate NF-κB expression in microglia and inhibit their M1 polarization (28). To the best of our knowledge, however, whether PPF inhibits the NF-κB/NLRP3 pathway by regulating MFG-E8 expression, exerting neuroprotective effects in CIRI, has not been reported. The present study utilized oxygen-glucose deprivation/reoxygenation (OGD/R) BV2 microglial cell and transient middle cerebral artery occlusion (tMCAO) mouse models to investigate whether PPF inhibits pyroptosis mediated by the NF-κB/NLRP3 pathway by upregulating MFG-E8, thereby improving neuronal damage in CIRI.

Materials and methods

Construction of OGD/R cell models. Mouse microglial BV-2 (cat. no. SNL-155) and hippocampal neuronal HT22 (cat. no. SNL-202) cells were obtained from Wuhan Sunncell Biotechnology. Cells were cultured in BV-2 cell-specific medium (cat. no. SNLM-155) and HT22 cell-specific medium (SNLM-202; both Wuhan Sunncell Biotechnology, respectively. The cultures were maintained at 37˚C with 5% CO_2, and the medium was refreshed every 2 days.

Following normal culture for 24 h at 37˚C, BV-2 and HT22 cells were placed in a glucose- and serum-free basal medium (cat. no. PM150270, Wuhan Pricella Biotechnology) and placed in a 95% N_2, 5% CO_2 hypoxic incubator at 37˚C for 2 h. Cells were transferred to normal medium and maintained at 37˚C with 95% oxygen and 5% CO_2 for 24 h to construct an OGD/R cell model (29). In addition, for the PPF group, PPF (2, 4, 8, 16, 32, 64 and 128 μM, cat. no. HY-B0649, MedChemExpress) was added to the culture medium during reoxygenation (30). In subsequent experiments, cells were treated with 8, 16 and 32 μM PPF during reoxygenation to evaluate its neuroprotective effects. According to the method described by Beaulieu *et al* (31), OGD-treated HT22 (in the lower chamber) and BV2 cells (in the upper chamber) were co-cultured at 37˚C in a Transwell chamber (0.4 μm, Corning, Inc.) for 24 h at a 1:3 inoculation ratio of HT22:BV2 cells (Fig. 1A).

Cell transfection. MFG-E8 small interfering (si)RNA (forward, 5'-CCAAUGUCUGGUGACUUUTT-3' and reverse, 5'-AAA GUCACCAGACAUUUGGTT-3'), MFG-E8 overexpression (OE) plasmid and negative control plasmids (si-NC: Forward, 5'-GAUGGAGAAGCUCGCUGATTT-3' and reverse, 5'-AAA UCAGCGAGCUUCUCCATT'; OE-NC) were synthesized by Sangon Biotech Co., Ltd. Plasmids (2 μg) were transfected into BV-2 cells for 48 h at 37˚C using Lipofectamine 3000 (Invitrogen; Thermo Fisher Scientific, Inc.) according to the manufacturer's instructions. At 48 h post-transfection, BV-2 cells were fully lysed with RIPA lysis buffer (cat. no. 20-188, Sigma-Aldrich; Merck KGaA) and MFG-E8 protein expression was analyzed by western blotting to evaluate the transfection efficiency. For the OGD/R + OE-MFG-E8 + LPS (NF-κB agonist) group, cells were transfected with OE-MFG-E8, treated with OGD and exposed to LPS (1 μg/ml; cat. no. HY-D1056, MedChemExpress) during reoxygenation (32). For the OGD/R + si-MFG-E8 + PPF group, BV-2 cells were first transfected with si-MFG-E8, then subjected to OGD and treated with PPF during reoxygenation.

Cell Counting Kit-8 (CCK-8) assay. BV-2 and HT22 cells were inoculated into 96-well plates ($1x10^4$ cells/well, 100 μl). When the cells were completely adherent (12-16 h), PPF (2, 4, 8, 16, 32, 64 and 128 μM) or LPS (0.125, 0.250, 0.500, 1.000 and 2.000 μg/ml) were added for another 24 h at 37˚C. The wells received 10% CCK-8 reagent (cat. no. HY-K0301, MedChemExpress), which was then thoroughly mixed and incubated in the dark for 2 h. Finally, the optical density at 450 nm (OD_{450}) was assessed by SpectraMax Mini microplate reader (Molecular Devices, LLC) to calculate cell viability.

Flow cytometry. BV-2 cells were resuspended with PBS to prepare a single cell suspension with a concentration of $1.0x10^7$ cells/ml. Anti-CD86 (1:100, cat. no. MA5-52361), anti-CD11b (1:100, cat. no. PA5-79533) and anti-CD206 antibody (1:400, cat. no. 17-2061-82; all Invitrogen; Thermo Fisher Scientific, Inc.) were added for 30 min under dark conditions at 4˚C. Samples were detected with BD FACSCalibur flow cytometer and the FlowJo software (v10.8l; both BD Biosciences) for analysis.

Calcein AM/PI staining. The viability of HT22 cells was assessed by Calcein AM/PI detection kit (cat. no. C2015M, Beyotime Biotechnology). HT22 cells were washed with PBS,

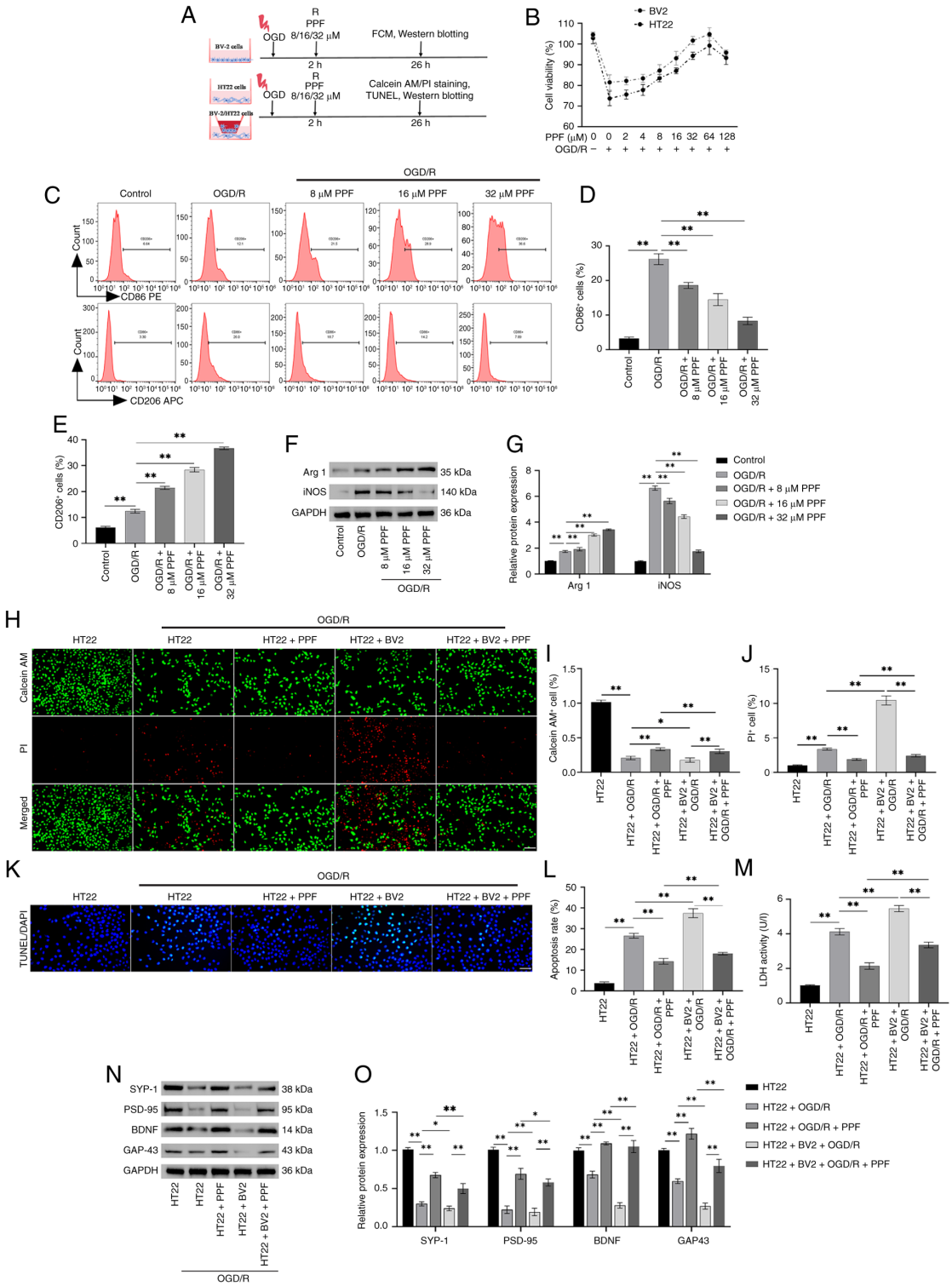

Figure 1. PPF suppresses excessive activation of BV-2 cells and ameliorates damage in HT22 cells following OGD/R. (A) Operational flowchart. (B) Cell Counting Kit-8 assay was performed to determine the viability of BV2 and HT22 cells after 24 h treatment with PPF. (C) Flow cytometry revealed that PPF decreased the number of CD86-positive and increased the number of CD206-positive cells. (D) Quantitative analysis of flow cytometry confirmed that PPF significantly decreased the proportion of CD86-positive cells and (E) significantly increased the proportion of CD206-positive cells. (F) Western blotting of iNOS, Arg 1, and GAPDH (internal reference). (G) Western blotting revealed that PPF decreased iNOS and increased Arg 1 levels in BV-2 cells. (H) Calcein AM/PI staining revealed decreased viability in OGD/R-treated HT22 cells, which was diminished upon co-culture with BV-2 cells, whereas PPF enhanced cell survival (magnification, x20; scale bar, 100 μm). (I) Quantitative analysis of Calcein AM/PI staining showed that PPF enhanced the survival ability of HT22 cells in the OGD/R+BV2 co-culture system and (J) decreased the death rate of HT22 cells in the OGD/R+BV2 co-culture system. (K) TUNEL staining to assess TUNEL positivity in HT22 cells (green fluorescence) (magnification, x40; scale bar, 50 μm). (L) TUNEL staining indicated increased apoptosis in OGD/R-treated HT22 cells. Co-culture with BV-2 cells elevated apoptosis rates, whereas PPF reduced apoptosis. (M) Following OGD/R, LDH release increased in HT22 cells and was further elevated after co-culture with BV-2 cells, while PPF treatment decreased LDH release. (N) Western blotting protein bands for SYP-1, PSD-95, BDNF, GAP-43, and GAPDH. (O) Quantitative analysis of western blotting revealed that PPF induced elevated SYP-1, PSD-95, BDNF and GAP-43 levels in HT22 cells. *P<0.05, **P<0.01. PPF, Propofol; OGD/R, Oxygen-glucose deprivation/reoxygenation; iNOS, inducible nitric oxide synthase; Arg, arginase 1; LDH, lactate dehydrogenase; SYP, synapsin; PSD, postsynaptic density protein; BDNF, brain-derived neurotrophic factor; GAP, growth-associated protein; FCM, flow cytometry.

mixed with Calcein AM/PI detection working solution (500 μl) and incubated at 37˚C for 30 min in a dark environment. Following incubation, staining was observed by fluorescence microscope (cat. no. BZ-X810, Keyence Corporation). Live (green) and dead (red) cell counts were analyzed using ImageJ 1.54h software (National Institutes of Health).

TUNEL staining. HT22 cells were plated into 12-well plates ($1.0x10^5$ cells/well, built-in sterile coverslip). Cells were exposed to 4% paraformaldehyde (cat. no. 441244, Sigma-Aldrich; Merck KGaA) to fix the cells for 30 min at 25˚C. 0.3% Triton X-100 solution (cat. no. T824275, Shanghai Macklin Biochemical Co., Ltd.) was added at 25˚C for 10 min to increase permeability. TUNEL detection solution (cat. no. C1086, Beyotime Biotechnology) was added for 60 min at 37˚C in a dark environment, then rinsed three times with PBS. The cells were incubated with DAPI (1 μg/ml, cat. no. D669617, Shanghai Macklin Biochemical Co., Ltd.) at 25˚C for 5 min in the dark to stain cell nuclei, followed by three additional rinses with PBS. Once sealed with Anti-fade Mounting Medium (cat. no. HY-K1047, MedChemExpress), samples were observed using a fluorescence microscope, and 5 non-overlapping random fields of view were captured per sample to assess the apoptosis rate using the ImageJ 1.54 h software.

Cell morphology observation. BV2 cells were mixed with glutaraldehyde solution (2.5%, cat. no. G6257, Sigma-Aldrich; Merck KGaA) and fixed in the dark at 4˚C for 4 h. After being washed twice with sterile PBS to remove glutaraldehyde, the samples were dehydrated with ethanol solution (30, 50, 70, 80, 90%) for 10 min each, then dehydrated with anhydrous ethanol. Finally, isoamyl acetate (cat. no. 79857, Sigma-Aldrich; Merck KGaA) was used to replace anhydrous ethanol twice, for 10 min each. After centrifugation at 1,000 x g, 4˚C for 5 min, the liquid was mixed with the cell pellet, and the mixture was dropped onto a silicon wafer, followed by drying at 37˚C. The dried sample was sputter-coated with gold for 150 sec and morphological observations and image capture were performed by scanning electron microscopy (SEM; cat. no. S-4800, Hitachi Ltd.).

Yo-Pro-1 and Hoechst 33342 staining. BV2 cells were seeded into a 12-well plate at a density of $1.0x10^5$ cells/well (built-in sterile coverslip). Cells were exposed to 4% paraformaldehyde for 30 min at 25˚C. Hoechst 33342 (cat. no. C1025) and Yo-Pro-1 staining solution (500 μl; cat. no. C1356S; both Beyotime Institute of Biotechnology) were added at 37˚C for 30 min. Cells were rinsed with PBS and photographed under a fluorescence microscope.

Caspase-1 enzyme activity assay. Caspase-1 enzyme activity was detected using the Caspase-1 Activity Assay kit (cat. no. E-CK-A381, Wuhan Elabscience Biotechnology) according to the manufacturer's instructions. BV2 cells (~$1x10^6$) were collected and washed with PBS. A total of 100 μl Cell Lysis Buffer was added in an ice bath for 30 min. The lysed samples were centrifuged at 8,000 x g for 10 min at 4˚C and the protein concentration in the supernatant was assayed by the BCA Protein Quantification kit. A total of 50 μl lysate was added to 45 μl Reaction Buffer and 5 μl Ac-YVAD-pNA were added for 2 h at 37˚C. OD_{405} was measured using a microplate reader and enzyme activity was calculated.

Dual-luciferase reporter assay. Wild-type (WT) and mutant-type (MUT) dual luciferase reporter plasmids for the NF-κB 3' untranslated region were synthesized by Sangon Biotech Co., Ltd. NF-κB-WT and si-MFG-E8, NF-κB-WT and si-NC, NF-κB-MUT, si-MFG-E8, and NF-κB-MUT and si-MFG-E8, respectively, were co-transfected into BV2 cells using Lipofectamine 3000 as aforementioned. Cells were collected after 48 h and assayed for luciferase activity using the Dual-Lucy Assay kit (cat. no. RG027, Beyotime Biotechnology) as previously described (33). Firefly luciferase activity was normalized to *Renilla* luciferase activity.

Construction of tMCAO mouse model. A total of 63 male C57BL/6 mice (age, 3 months; weight, 21-24 g) was obtained from Beijing Vital River Laboratory Animal Technology Co., Ltd. and raised at 22˚C, humidity of 45-50%, 12/12-h light/dark cycle and food and water ad libitum. The mice were randomly divided into Sham (n=9) and experimental group (n=54) according to the random number table method. According to the method described by Liu *et al* (34), the tMCAO model was established. The mice received anesthesia with 2% isoflurane, followed by 1.5% isoflurane to maintain anesthesia and the surgical area was sterilized with 75% ethanol and 10% iodophor. In the experimental group, a small incision was made 4 mm from the bifurcation of right common carotid artery (CCA), with a suture placed around the internal carotid artery (ICA). The 0.16-mm diameter suture (cat. no. 1618-50, Beijing Cinontech Co., Ltd.) was gently pushed with ophthalmic tweezers, reaching an insertion depth of ~20 mm. The suture at the distal end of ICA and CCA was fastened to fix the suture. The incision was sutured and disinfected and a 6 mm suture was retained *in vitro* for reperfusion. After the blood supply was blocked for 45 min, the suture was removed. Blood flow in the mouse brain was monitored using Laser Speckle Doppler Flowmetry (PeriCam PSI Z; Perimed AB) (35). The body temperature of the mice was maintained at 37.0±0.5˚C using a homoeothermic blanket throughout the surgical process. Sham group mice were sutured and disinfected, but tMCAO was not performed. To reduce post-operative pain in mice, buprenorphine (0.1 mg/kg; cat. no. PHR8512; Sigma-Aldrich; Merck KGaA) was administered subcutaneously 15 min before and 12 h and once 24 h after surgery.

At 45 min after tMCAO, mice were injected intraperitoneally with normal saline or 50, 100 or 200 mg/kg PPF (n=9 mice/group) (36). In addition, for the tMCAO + 200 mg/kg PPF + si-MFG-E8 group or the tMCAO + 200 mg/kg PPF + si-NC group, mice were microinjected with si-MFG-E8 or si-NC (166.67 μM) intracerebrally 2 days prior to surgery and were injected intraperitoneally 45 min postoperatively with 200 mg/kg PPF (37). Mice were sacrificed 1 day after PPF administration. A double-blind method was used during the animal experiments; none of the researchers responsible for feeding the mice, behavioral scoring or histological analysis were aware of the grouping information.

Assessment of neurological deficit. At 24 h after tMCAO, Longa scoring method was used to determine whether the modeling was successful (38). The Longa score was determined as follows: 0, normal, no neurological deficit; 1, inability to fully extend the contralateral forepaw, mild neurological deficit; 2, turning to the paralyzed side when walking, moderate neurological deficit; 3, body tilting toward the paralyzed side when walking, severe neurological deficit; 4, inability to walk spontaneously, loss of consciousness. A score of 4 represents mice with irreversible severe cerebral ischemic damage or loss of consciousness, which prevented subsequent behavioral scoring (corner test). Therefore, a score of 1-3 points was judged as successful modeling.

At 24 h after tMCAO, the sensorimotor and postural asymmetry neurological functions of mice were detected by corner test (39). The mice were placed at the corner entrance between two plates connected at a 30˚ angle. Once the mouse reaches the corner, it will retreat and turn right or left. Each mouse was tested 20 times. If the mice did not retreat when turning around, the experiment was abandoned. The number of right and left turns was recorded.

Triphenyltetrazolium chloride (TTC) staining. Following behavioral testing, mice were sacrificed by intraperitoneal injection of sodium pentobarbital (100 mg/kg) for 1 min, with cardiac and respiratory arrest used to determine death. Mouse brain tissue was frozen at -80˚C for 20 min and sliced into 2-mm sections. Subsequently, the tissue sections were exposed to TTC solution (2%, cat. no. C0652, Beyotime Institute of Biotechnology) preheated to 37˚C and incubated in a dark environment for 15 min. Images were captured and the cerebral infarction volume was evaluated through ImageJ 1.54h software.

Brain water content detection. Brain tissue was washed with pre-cooled PBS, the surface liquid was dried by filter paper and immediately weighed. The weighed tissue was placed in a drying tube and placed in an oven at 100˚C for 24 h to dry (until the weight was constant) and weighed after cooling to room temperature. Brain water content (%) was calculated as follows: (Wet weight-dry weight)/wet weight x100%.

Hematoxylin and eosin (HE) staining. Brain tissue was exposed to 4% paraformaldehyde for 48 h at 4˚C, paraffin-embedded and serially sectioned (4 μm). The sections were dried and deparaffinized using xylene, then rehydrated using gradient ethanol. Following 10 min staining with hematoxylin, the sections were exposed to differentiation solution (cat. no. C0161s, Beyotime Institute of Biotechnology) for 30 sec. Sections were dyed with 1% eosin (cat. no. C0109, Beyotime Institute of Biotechnology) for 60 sec, dehydrated with gradient ethanol, transparentized with xylene and covered with neutral balsam. The ischemic penumbra was evaluated using a light microscope (Leica GmbH).

Nissl staining. Brain tissue was exposed to 4% paraformaldehyde for 48 h at 4˚C, paraffin-embedded and serially sectioned (4 μm), and then placed in warm water to expand. The slices were placed in a drying oven at 65˚C for 90 min, dewaxed with xylene for 20 min and rehydrated in gradient ethanol. The liquid was removed, and sections were exposed to Nissl staining solution (cat. no. C0117, Beyotime Institute of Biotechnology) for 10 min at 25˚C. After rinsing with tap water, tissue was immersed in 95% ethanol for dehydration for 4 min, then xylene. Following sealing with neutral balsam, samples were visualized with an inverted light microscope.

Fluoro-Jade C (FJC) staining. As described by Liu *et al* (34), the FJC degenerated neuron staining kit (cat. no. TR-100-FJT, Wuhan Anjiekai Biological Medicine Technology Co., Ltd.) was used to evaluate the neuronal degeneration in mice. The frozen sections of mouse brain tissue were treated with NaOH/ethanol solution (1:10) for dehydration for 4 min at 25˚C, then treated with potassium permanganate (1:10 dilution) for 10 min at 25˚C to enhance reagent permeability. Sections were then stained with FJC solution (1:10) in darkness for 10 min at 25˚C. Sections were sealed with Anti-fade mounting medium, observed by fluorescence microscope and the proportion of FJC-positive cells (degenerated neurons) was counted using ImageJ 1.54h software (National Institutes of Health).

Lactate dehydrogenase (LDH) assay. LDH is present in the cytoplasm and cannot penetrate the intact cell membrane. Therefore, the detection of LDH release can evaluate cell membrane damage (40). The release of LDH from HT22 cells was assessed using Cytotoxicity LDH assay kit (cat. no. HY-K1090, MedChemExpress). HT22 cells were centrifuged at 1,000 x g for 5 min at 4˚C, and 50 μl supernatant was mixed thoroughly with 50 μl LDH working solution. Following incubation in dark for 30 min at 25˚C, 50 μl Stop Solution was applied and OD_{490} value was detected immediately by microplate reader. In addition, the fresh brain tissue of mice was cut into pieces (~1 mm^3), mixed with PBS, homogenized, centrifuged at 8,000 x g for 10 min at 4˚C, and supernatant was mixed with LDH working solution. The LDH release in brain tissue was determined as aforementioned.

Immunofluorescence. Brain tissue was exposed to 4% paraformaldehyde for 48 h at 4˚C, paraffin-embedded and serially sectioned (4 μm). The paraffin sections of mouse brain tissue were dewaxed with xylene, hydrated in a descending anhydrous ethanol series. For antigen retrieval, sections were immersed in 0.01 M citrate buffer (pH 6.0) and heated in a microwave oven at 95˚C for 15 min, then naturally cooled to 25˚C and rinsed three times with PBS. Then, 0.3% Triton X-100 was dropped on the surface for 10 min and 5% bovine serum albumin (BSA; cat. no. ST023; Beyotime Biotechnology) was added for 1 h at 25˚C. Sections were exposed overnight to primary antibodies against Ionized calcium binding adaptor molecule 1 (Iba1, cat. no. PA5-27436, 1:500) and CD86 (cat. no. PA5-114995, 1:100) at 4˚C. The sections were rinsed in PBS and incubated with FITC- (cat. no. F-2765, 1:100) or Cy3-conjugated goat anti-rabbit IgG (cat. no. A10520, 1:100) in darkness for 1.5 h at 25˚C. All antibodies were obtained from Invitrogen (Thermo Fisher Scientific, Inc.). Following sealing with Anti-fade Mounting Medium, sections were observed by a fluorescence microscope and the fluorescence intensity was quantified using ImageJ 1.54h software.

BV2 cells were seeded in a 12-well plate ($1.0x10^5$ cells/well, coverslips were placed in the plate) for 24 h to make cell

climbing slides. The slides were exposed to paraformaldehyde for 20 min, rinsed with PBS and then incubated with 0.3% Triton X-100 at 25˚C for 10 min, blocked with BSA and exposed to primary antibodies against NLRP3 (cat. no. MA5-32255, 1:1,000) and apoptosis-associated speck-like protein containing a CARD (ASC, cat. no. PA5-50915, 1:200, Invitrogen; Thermo Fisher Scientific, Inc.) overnight at 4˚C. Subsequent immunofluorescence analysis was performed as aforementioned.

ELISA. Mouse TNF-α (cat. no. PT512), IL-10 (cat. no. PI522), IL-6 (cat. no. PI326), transforming growth factor-β (TGF-β; cat. no. PT878), IL-1β (cat. no. PI301), IL-18 (cat. no. PI553) and IFN-γ (cat. no.) PI508; all Beyotime Biotechnology) ELISA kits were used to evaluate inflammatory factors levels in mouse brain tissue and BV2 cells, according to the manufacturer's instructions. Mouse Claudin-5 (Cla; cat. no. CSB-EL005507MO; Cusabio Technology LLC), Occludin (Occ; cat. no. ml063481) and zona occludens 1 (ZO-1, cat. no. ml037693; both Shanghai Enzyme-linked Biotechnology Co., Ltd.) ELISA kits were used to evaluate the tight junction proteins in mouse brain tissue, according to the manufacturer's instructions. The target areas of brain tissue (ischemic penumbra and core area and non-ischemic area) were separated by a blade. The brain tissue homogenate or cell supernatant and corresponding antibody were added to the ELISA plate at 37˚C for 90 min. HRP-labeled streptavidin was introduced and incubated in the dark at 37˚C for 20 min. Chromogenic agent A and B were incubated for 15 min in a dark environment at 37˚C. Finally, 50 μl termination solution was introduced and mixed well to determine OD_{450} value.

Western blotting. The fresh brain tissue of the mice was cut into pieces and then RIPA lysis buffer (cat. no. 20-188, Sigma-Aldrich; Merck KGaA) was added. For BV2 cells, pre-cooled PBS was used for gentle washing twice and then RIPA lysis buffer was added for lysis. After lysis, the protein concentration was detected by the BCA protein quantification kit. A total of 30 μg protein/lane was loaded and separated by 10% SDS-PAGE, transferred onto PVDF membranes and blocked with 5% BSA at room temperature for 2 h. Following rinsing with TBST containing 0.1% Tween-20, the membrane underwent overnight incubation with primary antibodies against synapsin-1 (SYP-1, cat. no. 51-5200), inducible nitric oxide synthase (iNOS; cat. no. PA5-171061; both 1:1,000), arginase 1 (Arg 1, cat. no. PA5-29645, 1:5,000), postsynaptic density protein-95 (PSD-95; cat. no. 51-6900), brain-derived neurotrophic factor (BDNF; cat. no. PA5-85730; both 1:500), growth-associated protein 43 (GAP-43; cat. no. PA5-34943, 1:5,000), GSDMD (cat. no. PA5-116815; all Invitrogen; Thermo Fisher Scientific, Inc.), cleaved-caspase-1 (cat. no. HY-P80622; both 1:500, MedChemExpress), pro-caspase-1 (cat. no. PA5-87536, 1:2,000, Invitrogen; Thermo Fisher Scientific, Inc.), ASC (cat. no. ab283684), GSDMD-N (cat. no. ab215203; both 1:1,000; both Abcam), NLRP3 (cat. no. MA5-32255, 1:500), IL-1β (cat. no. P420B, 1:1,000), IL-18 (cat. no. PA5-79479, 1:2,000), phosphorylated (p-)NF-κB-p65 (cat. no. 44-711G, 1:1,000), MFG-E8 (cat. no. PA5-109955; all Invitrogen; Thermo Fisher Scientific, Inc.) and NF-κB-p65 (cat. no. ab76311; both 1:2,000, Abcam) at 4˚C. The membrane underwent incubation with goat anti-rabbit antibody (cat. no. 31460, 1:10,000, Invitrogen; Thermo Fisher Scientific, Inc.) for 2 h at 25˚C. Subsequently, the ECL working solution (cat. no. HY-K1005, MedChemExpress) was prepared and uniformly dropped onto the membrane, which was scanned using iBright CL1500 gel imaging system (Invitrogen; Thermo Fisher Scientific, Inc.). After scanning, the gray value was determined with ImageJ 1.54h software and normalized to GAPDH (cat. no. PA1-987, 1:1,000, Invitrogen; Thermo Fisher Scientific, Inc.).

Statistical analysis. All data are presented as the mean ± standard deviation of ≥3 independent experimental repeats. SPSS 26.0 software (IBM Corp.) was employed for statistical analysis. $P<0.05$ was considered to indicate a statistically significant difference. Prism software (GraphPad 9.0; Dotmatics) was used for plotting. The results were analyzed via unpaired t-test or one-way ANOVA with post hoc Tukey's test.

Results

PPF suppresses excessive activation of BV-2 cells and ameliorates damage in HT22 cells following OGD/R. The present study reoxygenated BV-2/HT22 cells in the presence of PPF following OGD. BV-2 and HT22 cell viability markedly declined following OGD/R, as indicated by CCK-8 assay (Fig. 1B). PPF (2-64 μM) increased cell viability, but viability decreased at 128 μM PPF (Fig. 1B). In subsequent experiments, cells were treated with 8, 16 and 32 μM PPF to evaluate its neuroprotective effects. Flow cytometry revealed that following OGD/R, CD86 (a marker of M1-type microglia) positivity increased in BV-2 cells, accompanied by a significant rise in CD206-positive cells (a marker of M2-type microglia) Following PPF treatment, the number of CD86-positive cells decreased significantly, while CD206-positive cells increased significantly, suggesting that PPF regulated the phenotypic conversion of BV-2 cells (Fig. 1C-E). Western blotting verified that PPF decreased iNOS (an M1-type marker) protein levels in BV-2 cells while upregulating Arg 1 (an M2-type marker), consistent with flow cytometry findings (Fig. 1F and G). OGD/R-treated HT22 cells were co-cultured with BV-2 cells to simulate neuroglial interactions. Calcein AM/PI dual staining demonstrated that HT22 cell viability decreased notably following OGD/R treatment. When HT22 cells were co-cultured with BV-2 cells, their survival rate decreased further. PPF treatment effectively reversed this trend, increasing the proportion of viable HT22 cells (Fig. 1H-J). TUNEL staining revealed that OGD/R treatment significantly increased apoptosis in HT22 cells, with further elevation following co-culture with BV-2 cells (Fig. 1K and L). PPF treatment significantly decreased apoptosis in HT22 cells (Fig. 1K and L). Following OGD/R, LDH release in HT22 cells significantly increased. Co-culture with BV-2 cells further elevated LDH release, indicating exacerbated cell damage. PPF treatment markedly decreased LDH release, suggesting its protective effect on HT22 cells (Fig. 1M). In addition, PPF increased the levels of SYP-1, PSD-95, BDNF and GAP-43 in HT22 cells, suggesting synaptic function maintenance and neural repair in HT22 cells (Fig. 1N and O). The results indicate

that PPF suppressed OGD/R-induced excessive activation in BV-2 cells, mitigated damage to HT22 cells and upregulated the expression of neurofunction-related proteins.

PPF suppresses NLRP3-mediated pyroptosis in BV2 cells following OGD/R. SEM revealed that following OGD/R, BV2 cells exhibited typical pyroptotic features, such as marked cellular swelling, irregular morphology, membrane pores and cytoplasmic contents leakage. Following PPF, the aforementioned morphological abnormalities in BV2 cells were attenuated (Fig. 2A). The levels of pyroptosis were assessed using Yo-Pro-1 and Hoechst 33342 staining. Following OGD/R, Yo-Pro-1-positive staining in BV2 cells was markedly increased, while PPF treatment decreased the number of Yo-Pro-1-positive cells (Fig. 2B and C). Immunofluorescence analysis revealed increased fluorescence intensity of NLRP3 and ASC following OGD/R, whereas PPF decreased the fluorescence intensity of both proteins in BV2 cells (Fig. 2D-F). Caspase-1 activity was significantly elevated in BV2 cells following OGD/R, whereas PPF decreased its activity (Fig. 2G). Moreover, following OGD/R, the protein levels of cleaved-caspase-1/pro-caspase-1, GSDMD-N/GSDMD, NLRP3, IL-1β, ASC, and IL-18 were markedly elevated in BV2 cells. By contrast, PPF lowered protein levels, suggesting that PPF inhibited NLRP3 inflammasome activation (Fig. 2H-K). ELISA showed that the levels of IL-1β and IL-18 in BV2 cells were significantly elevated following OGD/R, and PPF treatment decreased the levels of both (Fig. 2L). These results indicated that PPF suppresses NLRP3 inflammasome activation following OGD/R, thereby inhibiting pyroptosis in BV2 cells.

OE-MFG-E8 suppresses OGD/R-induced NF-κB and NLRP3 activation in BV2 cells. Previous studies have revealed that MFG-E8 is key in microglial inflammation (18,41). To investigate the impact of MFG-E8 on NF-κB signaling and NLRP3 activation, OE-MFG-E8 was transfected into BV2 cells, followed by OGD/R. Following OGD/R, MFG-E8 expression decreased in BV2 cells, while p-NF-κB/NF-κB levels increased, suggesting that OGD/R may downregulate MFG-E8 and activate NF-κB signaling (Fig. 3A-C). Transfection of BV2 cells with OE-MFG-E8 significantly elevated MFG-E8 protein levels, confirming successful establishment of the model (Fig. 3D and E). Following transfection with OE-MFG-E8, p-NF-κB/NF-κB, NLRP3 and ASC expression notably declined in BV2 cells (Fig. 3F-H). The present study examined the effects of different concentrations of NF-κB activator LPS on the protein levels of the NF-κB pathway in microglia and found that 0.25-2.00 μg/ml LPS effectively reduced p-NF-κB/NF-κB ratio (Fig. S1A and B). Additionally, LPS at 0.125-1.000 μg/ml had no adverse effect on BV-2 cell viability (Fig. S1C), therefore 1 μg/ml LPS was selected for subsequent experiments. The p-NF-κB/NF-κB, NLRP3 and ASC levels were significantly elevated in BV-2 cells following LPS treatment (Fig. 3I-K). Overexpression of MFG-E8 significantly decreased p-NF-κB/NF-κB levels in OGD/R-treated BV2 cells, whereas LPS increased p-NF-κB/NF-κB levels (Fig. 3L and M). Following OGD/R, immunofluorescence indicated increased fluorescence intensity of ASC and NLRP3 in BV2 cells. OE-MFG-E8 decreased the fluorescence intensity of both proteins, whereas LPS attenuated the effect of OE-MFG-E8 (Fig. 3N-P). In addition, following MFG-E8 overexpression, cleaved-caspase-1/pro-caspase-1, NLRP3, ASC, IL-1β, GSDMD-N/GSDMD and IL-18 protein levels were reduced notably in OGD/R-treated BV2 cells. However, LPS inhibited the impact of OE-MFG-E8 overexpression (Fig. 3Q-T). The results indicated that OE-MFG-E8 suppresses NF-κB signaling and NLRP3 activation in OGD/R-induced BV2 cells.

PPF suppresses pyroptosis induced by NF-κB/NLRP3 signaling by upregulating MFG-E8. The present study investigated whether PPF inhibits pyroptosis by regulating MFG-E8 in BV-2 cells. si-MFG-E8 was transfected into BV-2 cells, which were subjected to OGD/R and exposed to PPF for 24 h. PPF treatment significantly increased MFG-E8 expression in BV2 cells, while simultaneously decreasing p-NF-κB/NF-κB levels, suggesting that PPF may inhibit NF-κB activation by upregulating MFG-E8 (Fig. 4A-C). Following transfection with si-MFG-E8, MFG-E8 protein expression markedly declined in BV2 cells, indicating successful establishment of MFG-E8 silencing (Fig. 4D and E). Silencing MFG-E8 significantly increased the luciferase activity of NF-κB-WT but had no significant effect on NF-κB-MUT, confirming that NF-κB was a downstream target of MFG-E8 (Fig. 4F). si-MFG-E8 attenuated the impact of PPF, causing a notable rise in p-NF-κB/NF-κB levels. This indicated that the inhibitory impact of PPF on NF-κB activation was dependent on MFG-E8 (Fig. 4G and H). PPF treatment significantly reduced the number of Yo-Pro-1-positive BV2 cells following OGD/R, whereas MFG-E8 silencing led to an increase in Yo-Pro-1 positivity, indicating that si-MFG-E8 attenuated the inhibitory effect of PPF on pyroptosis (Fig. 4I and J). ELISA revealed that levels of proinflammatory factors TNF-α, IL-1β and IL-6 were markedly raised in BV2 cells following OGD/R, while IL-10 levels decreased. PPF treatment reversed this effect, whereas silencing MFG-E8 attenuated the anti-inflammatory effect of PPF (Fig. 4K-N). Additionally, PPF markedly decreased cleaved-caspase-1/pro-caspase-1, NLRP3, ASC, IL-1β, GSDMD-N/GSDMD and IL-18 levels in OGD/R-treated BV2 cells, whereas si-MFG-E8 markedly increased these protein levels (Fig. 4O-R). These results suggested that PPF suppresses pyroptosis by upregulating MFG-E8 in BV2 cells, thereby inhibiting NF-κB/NLRP3 pathway activation.

PPF improves neurological deficit and reduces brain tissue pathology in tMCAO mice. The present study established a tMCAO mouse model to investigate whether PPF effectively improves neuronal injury *in vivo* (Fig. 5A). The Longa scoring system results demonstrated that neurological deficit scores were significantly lower in the PPF-treated group compared with the tMCAO group, indicating that PPF improved neurological function in tMCAO mice (Fig. 5B). The corner test demonstrated that PPF effectively mitigated sensorimotor deficits in tMCAO mice, reduced turning bias and enhanced limb coordination and spatial perception (Fig. 5C). Moreover, PPF significantly reduced brain tissue water content in tMCAO mice, indicating that PPF alleviated ischemia-induced cerebral edema (Fig. 5D). TTC staining revealed well-defined white infarct lesions in the cerebral cortex of tMCAO mice.

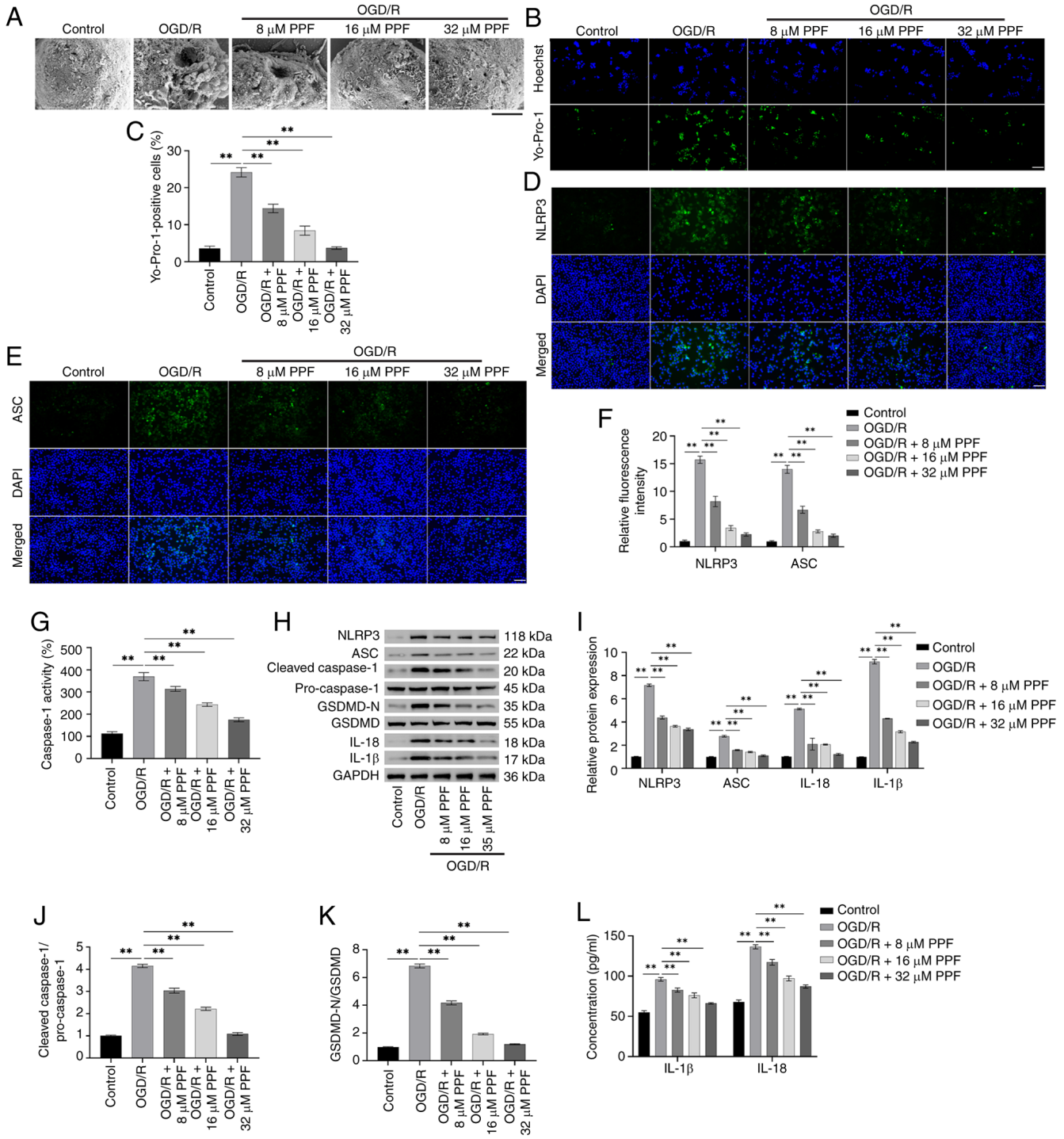

Figure 2. PPF suppresses NLRP3-mediated pyroptosis in BV2 cells following OGD/R. (A) SEM observation of BV2 cell morphology (magnification, x20,000; scale bar, 2 μm). (B) Yo-Pro-1 and Hoechst 33342 staining for assessing the pyroptosis levels in BV-2 cells. (C) Quantitative analysis of Yo-Pro-1 and Hoechst 33342 staining revealed that PPF deceased pyroptosis levels in BV-2 cells. (D) Immunofluorescence staining of NLRP3 in BV2 cells (magnification, x40; scale bar, 50 μm). (E) Immunofluorescence staining of ASC in BV2 cells (magnification, x40; scale bar, 50 μm). (F) Quantitative analysis of immunofluorescence staining revealed that NLRP3 and ASC fluorescence intensity increased in OGD/R-treated BV2 cells, while PPF decreased the fluorescence intensity of both proteins. (G) Caspase-1 activity was detected in BV2 cells following OGD/R using Caspase-1 Activity Assay kit. (H) Western blotting of NLRP3, ASC, cleaved-caspase-1, pro-caspase-1, GSDMD-N, GSDMD, IL-18, IL-1β, and GAPDH (internal reference). (I) Western blot analysis revealed elevated NLRP3, ASC, IL-1β and IL-18, cleaved-caspase-1/pro-caspase-1 levels (J), and GSDMD-N/GSDMD levels (K) in OGD/R-treated BV2 cells, PPF treatment reduced these proteins levels. (L) ELISA showed that PPF decreased IL-1β and IL-18 levels. **P<0.01. PPF, Propofol; OGD/R, Oxygen-glucose deprivation/reoxygenation; ASC, apoptosis-associated speck-like protein containing a CARD; GSDMD, gasdermin D.

Following PPF treatment, the white infarct areas significantly decreased (Fig. 5E and F). HE staining revealed notable brain tissue damage in the penumbral region of tMCAO mice, characterized by disorganized cell arrangement and pronounced interstitial edema. PPF mitigated the extent of brain tissue damage (Fig. 5G). Nissl staining demonstrated a significant reduction in Nissl-positive cells within ischemic penumbra of tMCAO mice, indicating severe neuronal

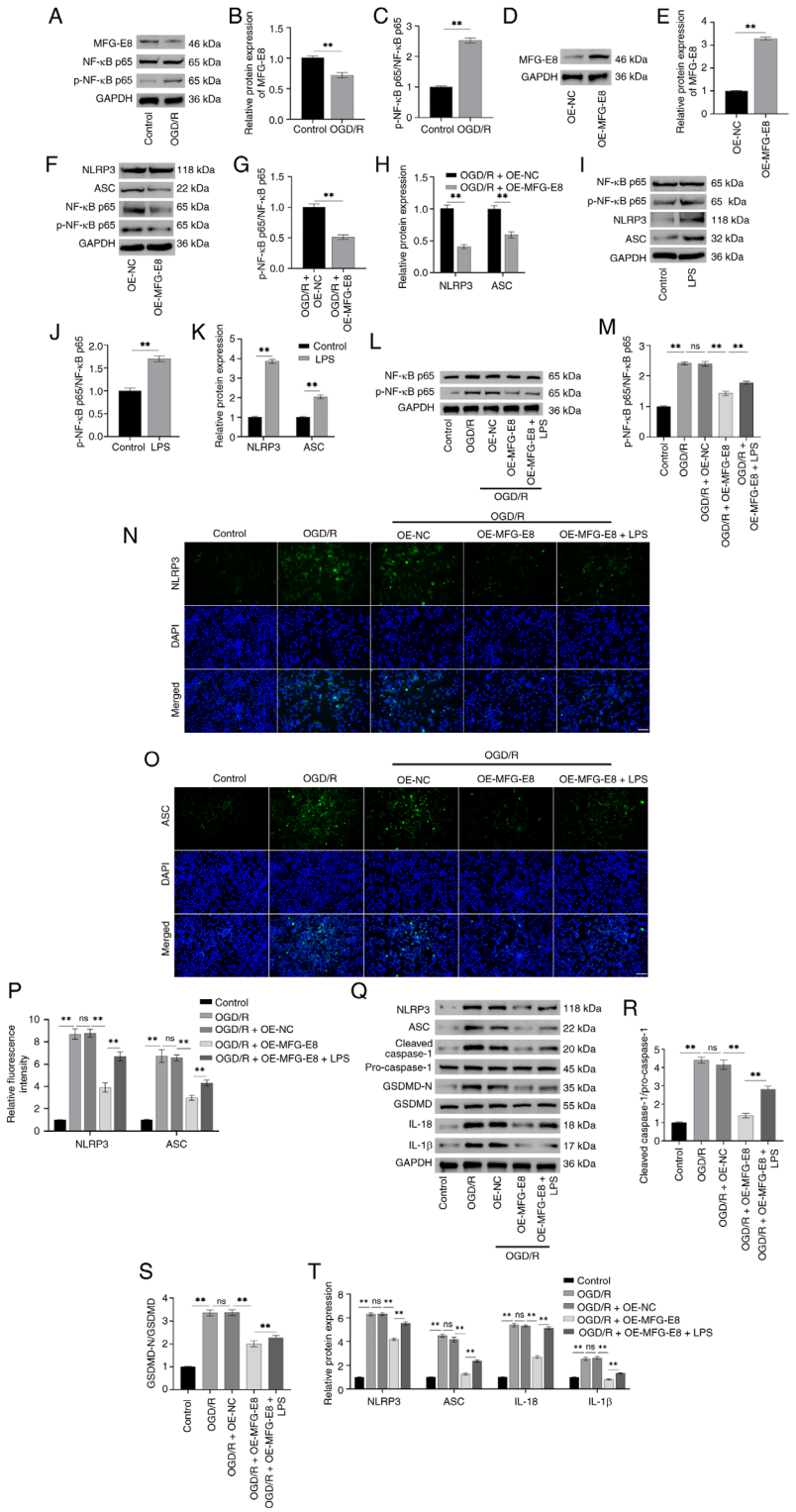

Figure 3. Overexpression of MFG-E8 suppresses NF-κB and NLRP3 activation in OGD/R-induced BV2 cells. (A) Western blotting protein bands for MFG-E8, p-NF-κB, NF-κB, and GAPDH (internal reference). (B and C) Following OGD/R, western blotting revealed decreased MFG-E8 expression (B) and elevated p-NF-κB/NF-κB levels (C) in BV2 cells. (D) Western blotting protein bands for MFG-E8 and GAPDH (internal reference). (E) Following transfection of OE-MFG-E8 into BV2 cells, MFG-E8 expression was elevated markedly. (F) Western blotting protein bands for NLRP3, ASC, p-NF-κB, NF-κB, and GAPDH (internal reference). (G and H) Following transfection with OE-MFG-E8, p-NF-κB/NF-κB levels (G), and NLRP3 and ASC levels (H) were detected using western blotting. (I) Western blotting protein bands for NLRP3, ASC, p-NF-κB, NF-κB, and GAPDH (internal reference). Following treatment with the NF-κB activator LPS, p-NF-κB/NF-κB (J), and NLRP3 and ASC levels (K) were detected by western blotting. (L) Western blotting protein bands for p-NF-κB, NF-κB, and GAPDH (internal reference). (M) Following transfection with OE-MFG-E8, p-NF-κB/NF-κB expression was decreased, whereas treatment with LPS increased p-NF-κB/NF-κB levels. (N) Immunofluorescence staining of NLRP3 in BV2 cells (magnification, x40; scale bar, 50 μm). (O) Immunofluorescence staining of ASC in BV2 cells (magnification, x40; scale bar, 50 μm). (P) Immunofluorescence revealed OE-MFG-E8 reduced the fluorescence intensity of NLRP3 and ASC, while LPS diminished the effect of MFG-E8 overexpression. (Q) Western blotting protein bands for NLRP3, ASC, cleaved-caspase-1, pro-caspase-1, GSDMD-N, GSDMD, IL-1β, IL-18, and GAPDH (internal reference). (R-T) Western blotting revealed that OE-MFG-E8 reduced cleaved-caspase-1/pro-caspase-1 levels (R), GSDMD-N/GSDMD levels (S), NLRP3, ASC, IL-1β, and IL-18 levels (T) in OGD/R-induced BV2 cells, LPS attenuated the impact of OE-MFG-E8. **P<0.01. PPF, Propofol; OGD/R, Oxygen-glucose deprivation/reoxygenation; ASC, apoptosis-associated speck-like protein containing a CARD; MFG-E8, milk fat globule-EGF factor 8; GSDM, gasdermin; OE, overexpression; p-, phosphorylated; LPS, lipopolysaccharide; NC, negative control; ns, not significant.

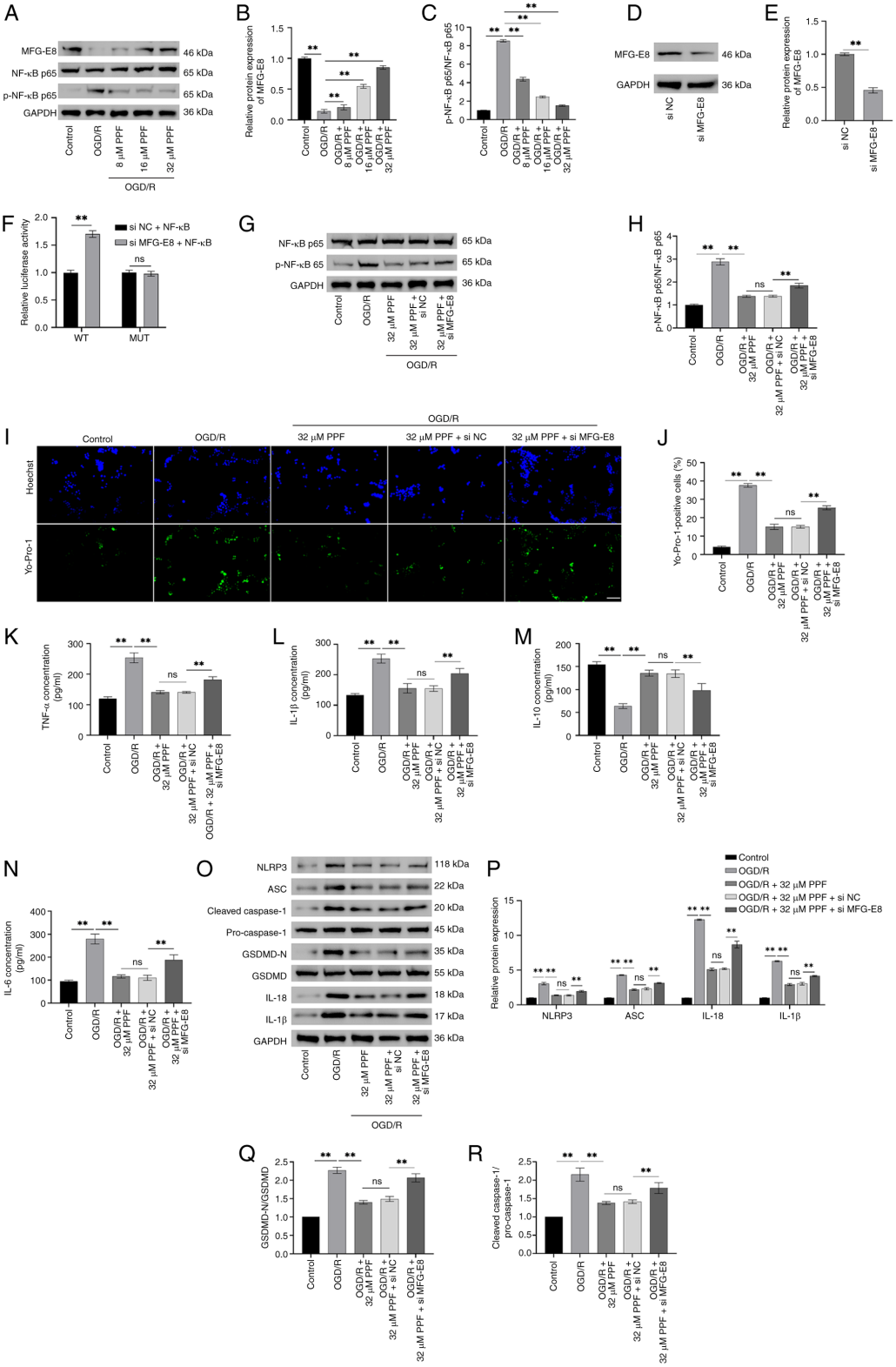

Figure 4. PPF suppresses pyroptosis caused by NF-κB/NLRP3 signaling by upregulating MFG-E8. (A) Western blotting protein bands for MFG-E8, p-NF-κB, NF-κB, and GAPDH (internal reference) in BV2 cells. (B) Western blotting revealed that PPF increased MFG-E8 and decreased p-NF-κB/NF-κB levels (C) in BV2 cells. (D) Western blotting for MFG-E8 and GAPDH in BV2 cells. (E) Following transfection of si-MFG-E8 into BV2 cells, MFG-E8 protein levels were significantly decreased. (F) Dual luciferase reporter gene assay confirmed that NF-κB is the target of MFG-E8. (G) Western blotting protein bands for p-NF-κB, NF-κB, and GAPDH (internal reference) in BV2 cells. (H) si-MFG-E8 attenuated the effects of PPF, resulting in elevated p-NF-κB/NF-κB levels. (I) Yo-Pro-1 and Hoechst 33342 staining for assessing the pyroptosis levels in BV-2 cells (magnification, x40; scale bar, 50 μm). (J) Yo-Pro-1 and Hoechst 33342 staining showed that PPF decreased Yo-Pro-1 positivity, while silencing MFG-E8 increased Yo-Pro-1 positivity. ELISA showed that PPF decreased TNF-α (K) and IL-1β (L) levels, silencing MFG-E8 reversed this effect. (M and N) ELISA showed that PPF raised IL-10 levels (M) and decreased IL-6 levels (N), silencing MFG-E8 reversed this effect. (O) Western blotting protein bands for NLRP3, ASC, cleaved-caspase-1, pro-caspase-1, GSDMD-N, GSDMD, IL-1β, IL-18, and GAPDH (internal reference) in BV2 cells. (P-R) Western blot analysis indicated that PPF decreased NLRP3, ASC, IL-1β, and IL-18 levels (P), GSDMD-N/GSDMD levels (Q), cleaved-caspase-1/pro-caspase-1 levels (R), silencing MFG-E8 increased these protein levels. **P<0.01. PPF, propofol; MFG-E8, milk fat globule-EGF factor 8; OGD/R, Oxygen-glucose deprivation/reoxygenation; ASC, apoptosis-associated speck-like protein containing a CARD; GSDM, gasdermin; OE, overexpression; p-, phosphorylated; LPS, lipopolysaccharide; NC, negative control; ns, not significant; si, small interfering; WT, wild-type; MUT, mutant.

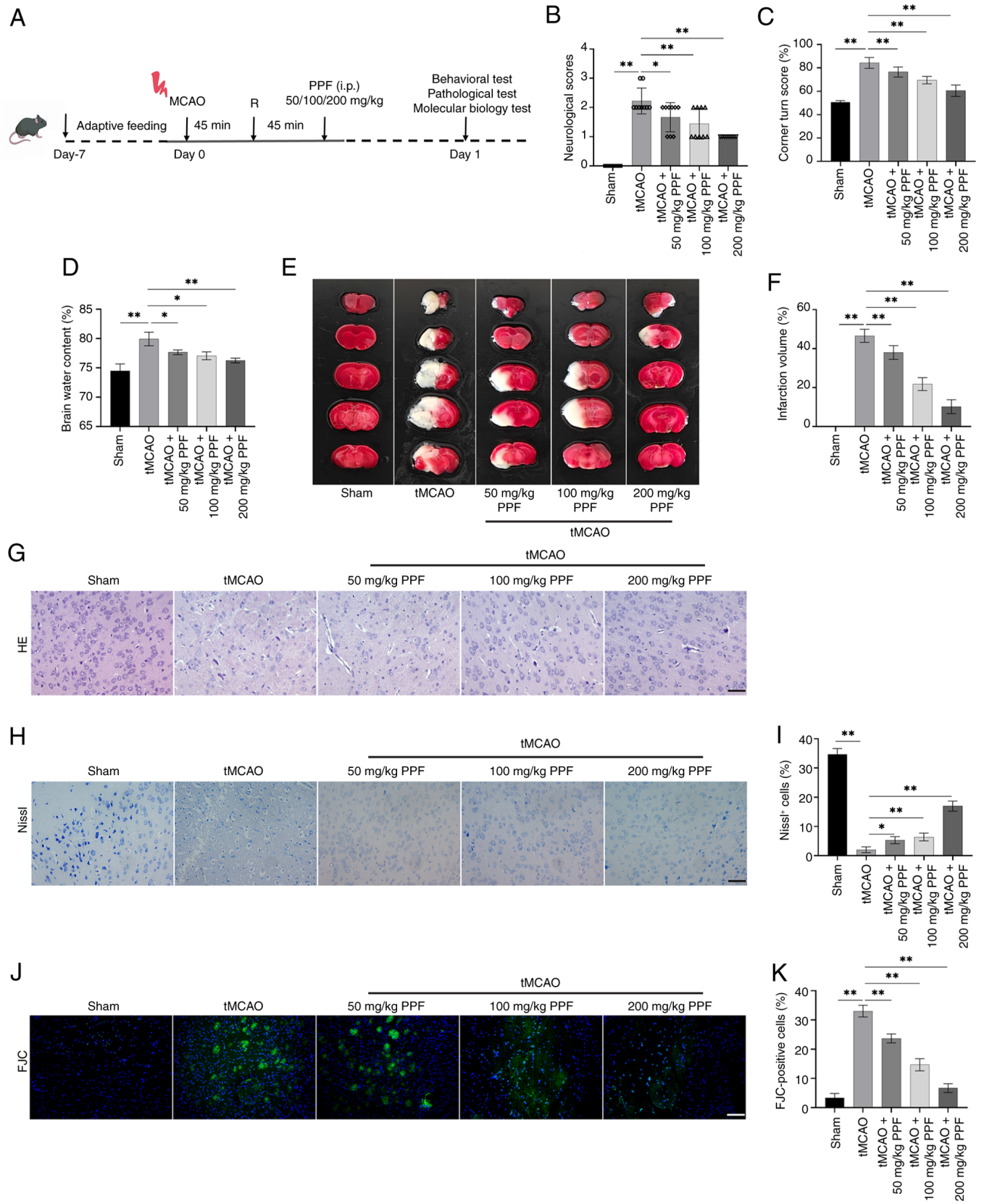

Figure 5. PPF improves neurological deficit and decreases brain tissue pathology in tMCAO mice. (A) Operational flowchart. (B) Longa scoring indicated that PPF decreased neurological deficit scores in tMCAO mice (n=9). (C) Corner test results demonstrated that PPF decreased sensorimotor deficits in tMCAO mice. (D) PPF decreased brain water content in tMCAO mice. (E) TTC staining to assess cerebral infarct lesions in tMCAO mice. (F) TTC staining revealed well-defined infarct lesions in the cerebral cortex of tMCAO mice, with PPF diminishing infarct volume. (G) HE staining was used to assess the histopathological brain damage in tMCAO mice (magnification, x40; scale bar, 50 μm). (H) Nissl staining was used to assess the proportion of Nissl-positive cells in the brain tissue of tMCAO mice (magnification, x40; scale bar, 50 μm). (I) Nissl staining revealed a decrease in Nissl-positive cell count in tMCAO mice. PPF increased the number of Nissl-positive cells. (J) Number of degenerative neurons in tMCAO mice was observed by FJC staining (magnification, x20; scale bar, 100 μm). (K) FJC staining indicated PPF decreased the number of degenerating neurons in the ischemic penumbra of tMCAO mice. *P<0.05, **P<0.01. PPF, Propofol; tMCAO, transient middle cerebral artery occlusion; HE, hematoxylin and eosin; FJC, Fluoro-Jade C; i.p., intraperitoneal injection.

damage. PPF markedly increased the number of Nissl-positive cells (Fig. 5H and I). Additionally, the number of FJC-positive degenerating neurons in the ischemic penumbra of tMCAO mice was markedly elevated. Following PPF treatment, the number of FJC-positive cells markedly declined, indicating that PPF suppressed neuronal degeneration following ischemia (Fig. 5J and K). The results indicate that PPF improves neurological deficits in tMCAO mice and effectively mitigated pathological damage in brain tissue.

PPF suppresses glial cell activation and neuronal injury in tMCAO mice. Immunofluorescence colocalization revealed a notably raised proportion of $CD86^+$ $Iba1^+$ cells in the ischemic penumbra of tMCAO mouse brains, suggesting a shift of microglia toward a proinflammatory phenotype (M1 type). Following PPF treatment, the proportion of $CD86^+$ $Iba1^+$ cells significantly decreased, indicating PPF suppressed proinflammatory activation of microglia in tMCAO mice after ischemia (Fig. 6A and B). In tMCAO mouse brain tissue, levels of proinflammatory factors (TNF-α, IFN-γ) were markedly raised in the ischemic core (Fig. 6C), penumbra (Fig. 6D) and non-ischemic regions (Fig. 6E), while anti-inflammatory factor (IL-10, TGF-β) levels notably decreased. PPF treatment reversed this phenomenon. LDH levels were markedly elevated in the ischemic penumbra of tMCAO mice, while PPF effectively decreased these levels, suggesting that PPF mitigated the extent of cellular damage (Fig. 6F). tMCAO mice exhibited significantly decreased levels of Cla, Occ, and ZO-1, whereas PPF markedly increased these tight junction protein levels, confirming its protective effect on the blood-brain barrier (BBB; Fig. 6G). Moreover, tMCAO mice exhibited significantly decreased levels of SYP-1 and PSD-95 in brain tissue and elevated levels of BDNF and GAP-43; PPF treatment reversed these effects (Fig. 6H and I). These results indicated that PPF alleviates neuronal injury by suppressing microglial activation in tMCAO mice, preserving BBB integrity and modulating the expression of proteins associated with neuronal function.

PPF upregulates MFG-E8 to hinder activation of the NF-κB/NLRP3 pathway. The present study investigated whether PPF exerts neuroprotective effects by regulating MFG-E8 expression, thereby identifying the key target of PPF intervention. MFG-E8 protein expression was notably decreased in tMCAO mice, whereas p-NF-κB/NF-κB levels were significantly elevated. Furthermore, NLRP3 inflammasome and pyroptosis-associated protein levels were markedly elevated. Following PPF treatment, MFG-E8 levels markedly elevated in the ischemic penumbra, while p-NF-κB/NF-κB and pyroptosis-associated protein levels significantly decreased. This indicated that PPF may suppress NF-κB/NLRP3 pathway activation and hinder pyroptosis by upregulating MFG-E8 (Fig. 7A-F). At 3 days after intracerebroventricular injection of si-MFG-E8, the expression of MFG-E8 protein in mouse brain tissue was significantly decreased (Fig. 7G and H). Additionally, MFG-E8 silencing markedly attenuated the protective impact of PPF on the ischemic penumbra in tMCAO mice. Compared with tMCAO + 200 mg/kg PPF +si NC group, p-NF-κB/NF-κB levels were elevated and cleaved-caspase-1/pro-caspase-1, NLRP3, ASC, IL-1β, GSDMD-N/GSDMD and IL-18 levels were markedly increased in tMCAO + 200 mg/kg PPF +si MFG-E8 group, confirming MFG-E8 as a key molecular target for PPF-mediated neuroprotective effects (Fig. 7I-N). These findings suggest that PPF suppressed abnormal activation of the NF-κB/NLRP3 pathway by upregulating MFG-E8, thereby decreasing pyroptosis. This may represent a key molecular mechanism underlying its neuroprotective effects.

Discussion

CIRI-mediated neuroinflammation is a key pathological mechanism in secondary brain injury. As crucial immune cells in the central nervous system, microglia are rapidly activated and polarized toward a pro-inflammatory phenotype (M1 type) following IRI. They release numerous pro-inflammatory factors, triggering an inflammatory storm that exacerbates neuronal damage (42,43). BV-2 cells are widely used as a classical microglia model *in vitro* to study the inflammatory mechanisms associated with ischemic brain injury (44,45). The key pathology of IRI is that ischemia-induced interruption of oxygen and glucose supply triggers cell hypoxic stress, which activates downstream inflammatory signaling pathways (46). The *in vitro* OGD/R model simulates this key pathological process, laying the foundation for *in vivo* experiments to explore the IR pathological process. The suture-based tMCAO model is considered the most representative surgical model for simulating human IS, offering advantages such as avoiding craniotomy, ease of operation and stable, controllable reperfusion (47,48). Based on the methods described by Liu *et al* (34) and Xu *et al* (29), the present study established OGD/R glial (BV-2) and hippocampal neuronal cell (HT22) models, as well as a tMCAO mouse model, to elucidate the neuroprotective effects of PPF in IS. Following OGD/R, BV2 cell viability decreased, M1 markers were highly expressed and their M1 polarization exacerbated apoptosis in HT22 cells following OGD/R, confirming the successful establishment of the OGD/R cell model. Furthermore, mice following tMCAO surgery exhibited pronounced neurological deficit and characteristic pathological lesions, including elevated neurological deficit score, enlarged infarct volume and increased numbers of degenerating neurons, indicating successful establishment of the tMCAO mouse model. PPF enhanced BV2 and HT22 cell viability following OGD/R, decreased LDH release, inhibited M1 polarization in BV2 cells and apoptosis in HT22 cells and decreased neurological deficit scores and cerebral infarct volume in tMCAO mice. Sun *et al* (17) confirmed that PPF can mitigate cortical damage in MCAO mice and decrease apoptosis in HT22 cells. These experimental findings collectively demonstrate that PPF improves neuronal injury, thus establishing a basis for deeper investigation into its neuroprotective effects. When the anti-inflammatory ability is enhanced, the expression of CD206 increases, while in a pro-inflammatory environment, the expression of CD86 increases. However, the OGD/R-induced double elevation in the present study suggests an imbalance between the over-activation of the M1 pathway and the pseudo-activation of the M2 pathway: On the one hand, OGD/R continuously activates the NF-κB/NLRP3 pathway through oxidative stress, leading to high CD86 expression and release of pro-inflammatory factors, triggering an excessive inflammatory response, whereas elevated

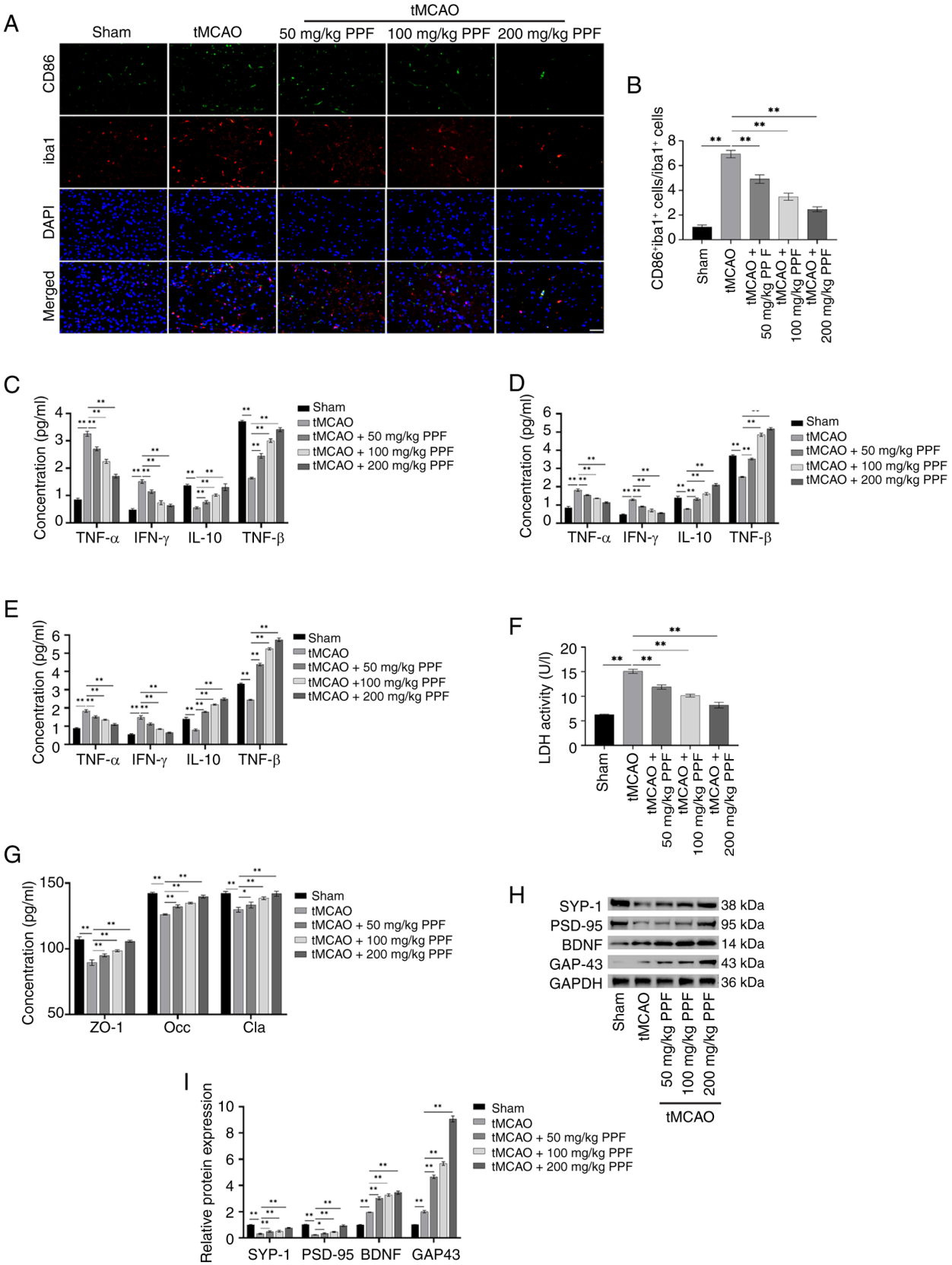

Figure 6. PPF suppresses microglial activation and neuronal injury in tMCAO mice. (A) Co-localization of Iba1 and CD86 was detected by immunofluorescence. (magnification, x40; scale bar, 50 μm). (B) Immunofluorescence colocalization revealed an increased proportion of CD86$^+$ Iba1$^+$ cells in tMCAO mice, which was decreased by PPF treatment. ELISA detection of TNF-α, IL-10, IFN-γ, and TGF-β levels in the ischemic (C) core and (D) penumbra and (E) non-ischemic zone of brain tissue. (F) Ischemic penumbra of tMCAO mice exhibited heightened LDH levels. PPF reduced LDH levels. (G) ELISA revealed decreased Cla, Occ and ZO-1 levels in tMCAO mice, while PPF elevated these tight junction-associated protein levels. (H) Western blotting of SYP-1, PSD-95, BDNF, GAP-43, and GAPDH (internal reference). (I) Western blotting revealed decreased SYP-1 and PSD-95 levels, along with increased BDNF and GAP-43 levels in tMCAO mice; these effects were reversed by PPF. *P<0.05, **P<0.01. PPF, Propofol; tMCAO, transient middle cerebral artery occlusion; Iba, Ionized calcium binding adaptor molecule; LDH, lactate dehydrogenase; Cla, Claudin; Occ, Occludin; ZO-1, zona occludens 1; PSD, postsynaptic density protein; BDNF, brain-derived neurotrophic factor; GAP, growth-associated protein; SYP, synapsin.

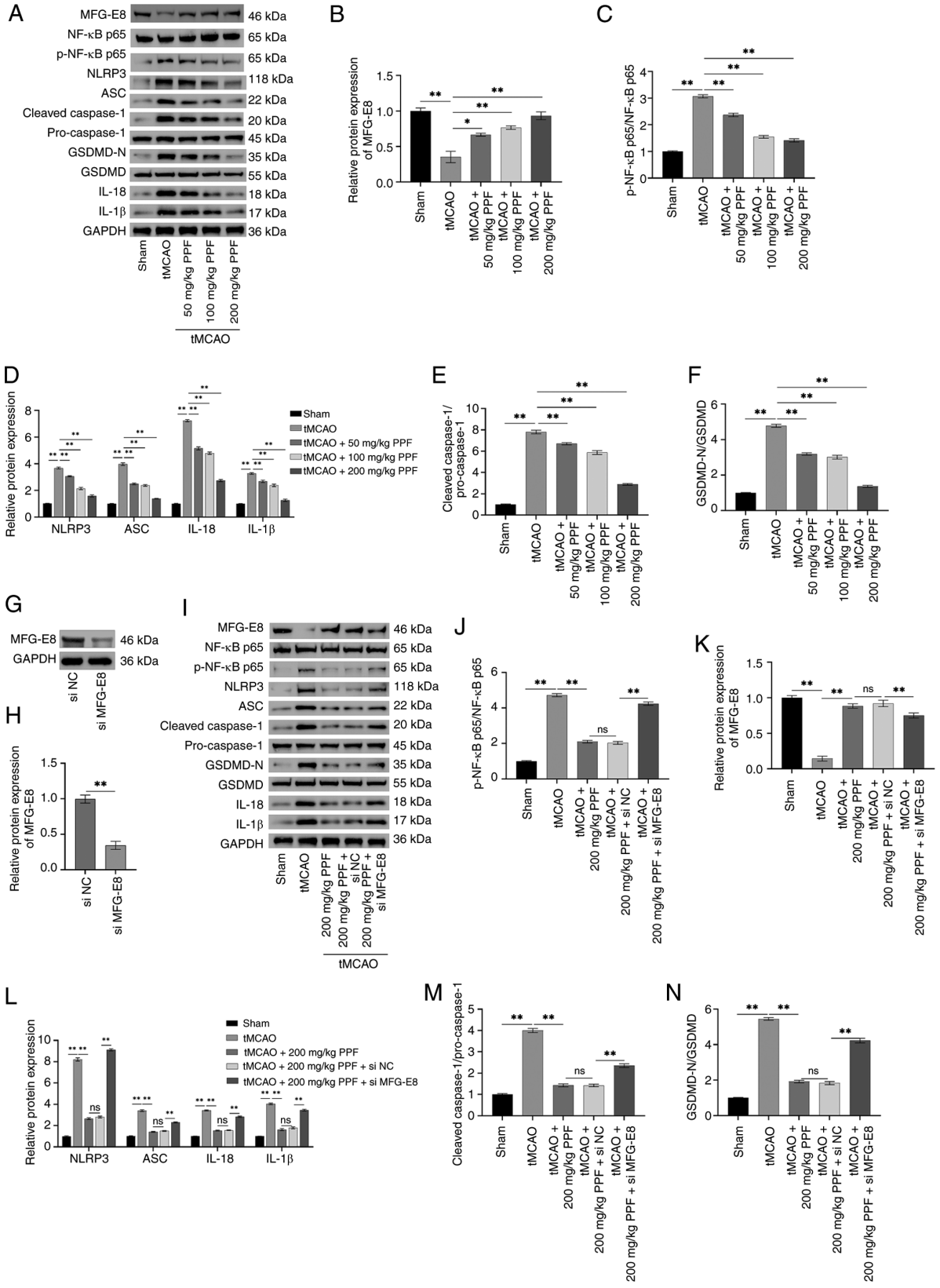

Figure 7. PPF upregulates MFG-E8 to inhibit activation of NF-κB/NLRP3 pathway. (A) Western blotting of MFG-E8, p-NF-κB, NF-κB, NLRP3, ASC, cleaved-caspase-1, pro-caspase-1, GSDMD-N, GSDMD, IL-18, IL-1β, and GAPDH (internal reference). (B-F) Western blot analysis revealed decreased MFG-E8 (B) levels in tMCAO mice, along with elevated p-NF-κB/NF-κB (C), NLRP3, ASC, IL-1β, IL-18 (D), cleaved-caspase-1/pro-caspase-1 (E), GSDMD-N/GSDMD (F) levels. PPF reduced these protein levels. (G) Western blotting protein bands for MFG-E8 and GAPDH (internal reference). (H) Western blotting detected the expression of MFG-E8 in the brain tissue of mice after injection of si-MFG-E8/si-NC. (I) Western blotting protein bands for MFG-E8, p-NF-κB, NF-κB, NLRP3, ASC, cleaved-caspase-1, pro-caspase-1, GSDMD-N, GSDMD, IL-18, IL-1β, and GAPDH (internal reference). (J-N) Western blot analysis revealed that si-MFG-E8 diminished the therapeutic efficacy of PPF, leading to deceased MFG-E8 level (J) and elevated p-NF-κB/NF-κB (K), NLRP3, ASC, IL-1β, and IL-18 levels (L), and cleaved-caspase-1/pro-caspase-1 (M) and GSDMD-N/GSDMD (N) levels in tMCAO mice. *P<0.05, **P<0.01. PPF, Propofol; tMCAO, transient middle cerebral artery occlusion; MFG-E8, milk fat globule-EGF factor 8; p-, phosphorylated; ASC, apoptosis-associated speck-like protein containing a CARD; ns, not significant; GSDMD, gasdermin D; si, small interfering; NC, negative control.

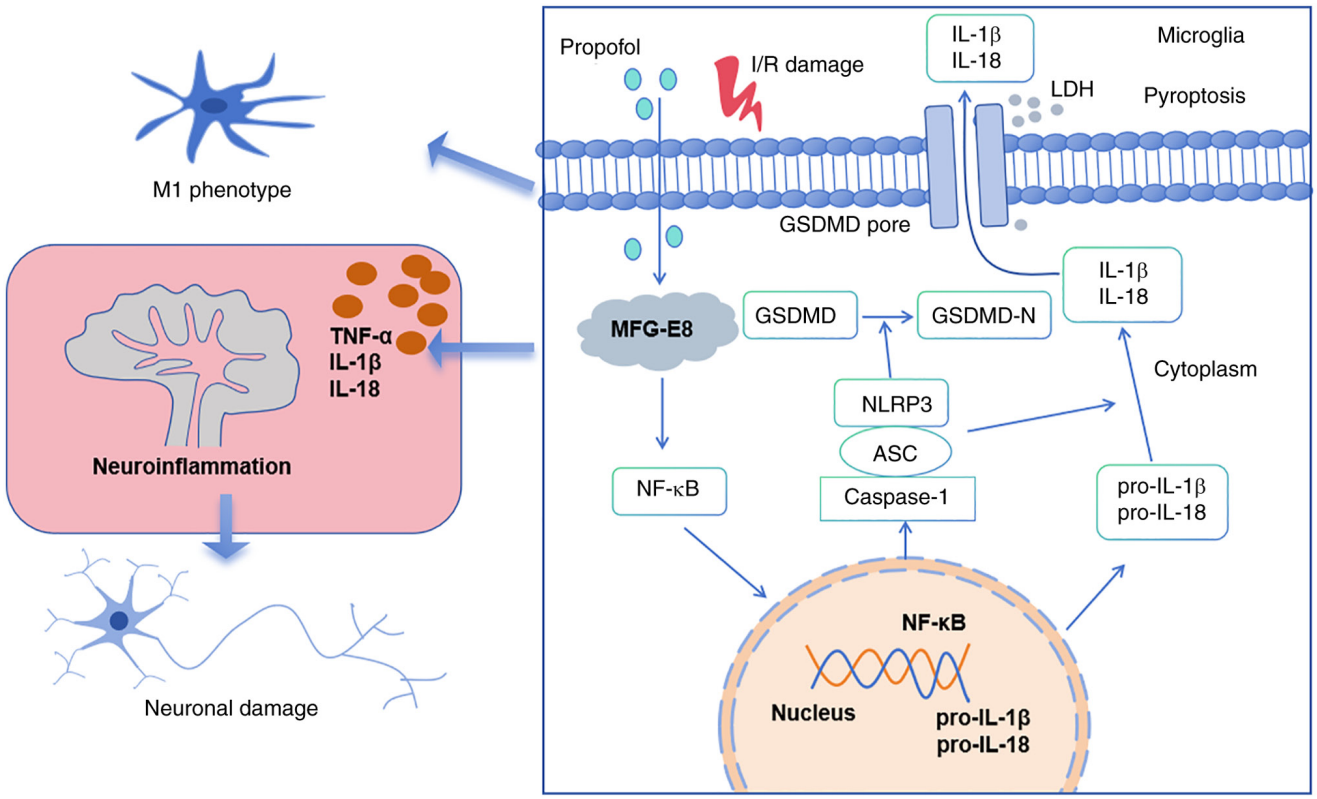

Figure 8. Mechanism of action of Propofol in attenuating I/R neuronal injury. Propofol ameliorates neuronal injury in cerebral I/R injury by inhibiting NF-κB/NLRP3 pathway-mediated focal death through upregulation of MFG-E8. I/R, ischemia/reperfusion; LDH, lactate dehydrogenase; GSDMD, gasdermin D; MFG-E8, milk fat globule-EGF factor 8; ASC, apoptosis-associated speck-like protein containing a CARD.

CD206 is a compensatory response for the body to initiate endogenous repair, but the repair effect of the M2 phenotype in this state is weak, as evidenced by the secretion of insufficient anti-inflammatory factors to inhibit inflammation or promote tissue repair (49). Under complex pathological stimuli such as hypoxia and trauma, microglia show co-expression of M1/M2 markers, but a pro-inflammatory phenotype (M1 type) predominates (9,50). In conclusion, the elevation of CD86 and CD206 after OGD/R is a phenotypic feature of microglia imbalance.

The ischemic brain injury zone is divided into two primary regions: Ischemic core and the penumbra (51). The ischemic core represents the area of most severe ischemic damage where brain cells have undergone irreversible necrotic death (52). The ischemic penumbra signifies the brain tissue located between the ischemic core and the normal area. If reperfusion therapy is administered promptly following ischemic injury, the neurons in the penumbra retain the potential for recovery (53,54). Therefore, preserving the survival of neurons and delaying damage progression are key strategies for treating IS. Given the clinical significance of the ischemic penumbra, the present study focused on the protective impact of PPF on neurons in the ischemic penumbra of tMCAO mice and its underlying mechanisms. Histopathological staining revealed that PPF increased the number of Nissl-positive neurons, decreased the number of degenerating neurons and suppressed pro-inflammatory microglia activation in the penumbra. This suggested that PPF effectively protected neurons in the ischemic penumbra. The BBB, as a key physiological barrier, typically restricts the migration of peripheral immune cells into brain parenchyma through its tight junction structure. Cerebral ischemia compromises the BBB, triggering immune cell infiltration and causing neuronal damage (55-57). Therefore, the present study evaluated the protective effect of PPF on the BBB. PPF effectively increased the tight junction-associated protein (Cla, Occ, and ZO-1) levels in the ischemic penumbra, indicating that PPF repaired the damaged BBB by upregulating these proteins. This may represent a key mechanism by which PPF decreases peripheral immune cell infiltration, alleviates neuroinflammation and protects neurons. Additionally, tMCAO-induced inflammatory response resulted in a significant decrease in SYP-1 and PSD-95 expression, reflecting the disruption of synaptic structure and loss of neurotransmission in the ischemic area. At the same time, the endogenous neuroprotective host self-protection mechanism is activated, which increases the expression of endogenous BDNF and promotes the repair of damaged neurons. However, this compensatory effect does not eliminate the neuronal damage caused by ischemia (58,59). The axonal regeneration marker GAP-43 also fails to form functional growth cones at damaged axon terminals to complete nerve loop reconstruction (60). Therefore, it was hypothesized that the increase in protein levels of BDNF and GAP-43 during the acute phase of tMCAO was a compensatory stress response.

MFG-E8, as a multifunctional glycoprotein, has drawn more interest in recent years for its role in nerve injury repair (61,62). Its key functions are in immune regulation, and maintenance of tissue homeostasis (61). Cheyuo *et al* (63) demonstrated that

MFG-E8 expression decreases in the brains of MCAO rats 24 h after ischemia, and injection of rhMFG-E8 decreases cerebral infarct volume and levels of necrotic neurons. In a hypoxic-ischemic encephalopathy rat model, MFG-E8 exhibits abnormal downregulation, treatment with MFG-E8-carrying exosomes decreases cerebral infarction volume by inhibiting autophagy and ferroptosis and alleviates cerebral edema in rats (62). The present study further validated this phenomenon: MFG-E8 levels notably declined in the ischemic penumbra of tMCAO mice and in BV2 cells following OGD/R. Conversely, PPF treatment induced a concentration-dependent upregulation of MFG-E8, suggesting that MFG-E8 may act as a key target for the neuroprotective effects of PPF. Cai *et al* (27) investigated resting microglia and found that PPF attenuates phagocytosis in resting BV2 cells by downregulating MFG-E8 expression. This suggests the regulatory effect of PPF on MFG-E8 may dynamically adjust according to the state of microglia. Future studies should investigate the differential regulatory mechanisms of the PPF/MFG-E8 pathway across different pathological stages or cell states.

Pyroptosis, also known as inflammatory necrosis, is distinguished by the breaking of the cell membrane and notable release of cell contents, thereby triggering a severe inflammatory response (64,65). IRI activates the NLRP3 inflammasome in microglia, triggering pyroptosis cascades that exacerbate neuroinflammation (66). Ruan *et al* (67) found that PPF protects lung tissue by suppressing proinflammatory factor secretion via downregulation of NLRP3. The present study also found that PPF inhibited NLRP3 activation, thereby suppressing microglial pyroptosis. In addition, the NF-κB pathway participates in NLRP3 activation and is associated with microglia M1 polarization; inhibiting NF-κB/NLRP3 pathway activation alleviates CIRI (68). Notably, OE-MFG-E8 in BV2 cells inhibited NF-κB signaling and suppressed NLRP3 activation. By contrast, following MFG-E8 silencing, the inhibitory effect of PPF on NF-κB/NLRP3 activation was diminished and both pyroptosis-associated marker and proinflammatory factor levels significantly increased. This implies that PPF may exert its neuroprotective effects by upregulating MFG-E8. In tMCAO mice, silencing MFG-E8 decreased the suppressive impact of PPF on NF-κB/NLRP3 activation, demonstrating that PPF blocks NF-κB/NLRP3 pathway activation by upregulating MFG-E8, thereby mitigating pyroptosis.

PPF serves a role in modulating the NF-κB/NLRP3 pathway in post-operative cognitive dysfunction rat model (69), and PPF has been shown to activate MFG-E8 (27). The present study demonstrated that PPF may play a role in attenuating CIRI by upregulating MFG-E8, thus modulating the NF-κB/NLRP3 pathway. More importantly, the present study revealed the activation pattern of microglia pyroptosis and polarization in CIRI, which provides a new theoretical basis for understanding the functional imbalance of microglia in complex pathological microenvironments and demonstrated that PPF has a dual protective effect: It directly acts on HT22 neurons to inhibit their apoptosis and regulate microglia pyroptosis and polarization and block the damage to neurons The present study provides more precise molecular targets for the development of IS therapeutic strategies targeting microglia.

The present study has certain limitations. Microglia and neurons from IRI model mice were not used in the *in vitro* experiments. Subsequent studies should isolate primary cells and validate them in combination with the *in vivo* tMCAO animal model to improve the reliability and translational value of findings. In addition, LPS induces the activation of multiple inflammatory pathways and validation experiments using TNF-α or Phorbol 12-myristate 13-acetate/ionomycin as NF-κB agonists should be conducted in the future. NLRP3 or GSDMD genes should be knocked down *in vitro* to directly validate their roles in the pyroptosis pathway.

PPF suppresses NF-κB pathway activation and downstream NLRP3-mediated pyroptosis by upregulating MFG-E8 expression, thereby alleviating CIRI (Fig. 8). PPF suppresses OGD/R-induced M1 activation and pyroptosis in BV2 cells, reduces proinflammatory factor release and improves HT22 neuronal survival. PPF alleviated neurological deficit in tMCAO mice, decreased infarct volume, protected the BBB and diminished neuronal degeneration. The present study revealed that PPF alleviates neuronal injury in CIRI by modulating the MFG-E8/NF-κB/NLRP3 pathway, providing potential therapeutic targets for CIRI. Future studies should investigate the role of PPF in CIRI animal models to elucidate its neuroprotective mechanisms.

Acknowledgements

Not applicable.

Funding

The present study was supported by National Key Research and Development Program Research on Prevention and Treatment of Common and High-Incidence Diseases Key Special Project 2021 Annual Project (grant no. 2021YFC2501100).

Availability of data and materials

The data generated in the present study may be requested from the corresponding author.

Authors' contributions

SG designed the study, performed experiments, interpreted data and edited the manuscript. YZ, GZ and ZZ interpreted data. All authors have read and approved the final manuscript. SG and ZZ confirm the authenticity of all the raw data.

Ethics approval and consent to participate

All animal experimental protocols were approved by the First Affiliated Hospital of Zhengzhou University Animal Welfare Committee (approval no. 2021090201; Henan, China).

Patient consent for publication

Not applicable.

Competing interests

The authors confirm that they have no competing interests.

References

1. Feigin VL, Brainin M, Norrving B, Martins SO, Pandian J, Lindsay P, F Grupper M and Rautalin I: World stroke organization: Global stroke fact sheet 2025. Int J Stroke 20: 132-144, 2025.
2. Tan KS, Pandian JD, Liu L, Toyoda K, Leung TWH, Uchiyama S, Kuroda S, Suwanwela NC, Aaron S, Chang HM and Venketasubramanian N: Stroke in Asia. Cerebrovasc Dis Extra 14: 58-75, 2024.
3. Li XY, Kong XM, Yang CH, Cheng ZF, Lv JJ, Guo H and Liu XH: Global, regional, and national burden of ischemic stroke, 1990-2021: An analysis of data from the global burden of disease study 2021. EClinicalMedicine 75: 102758, 2024.
4. Herpich F and Rincon F: Management of acute ischemic stroke. Crit Care Med 48: 1654-1663, 2020.
5. Feske SK: Ischemic stroke. Am J Med 134: 1457-1464, 2021.
6. Kapanova G, Tashenova G, Akhenbekova A, Tokpınar A and Yılmaz S: Cerebral ischemia reperfusion injury: From public health perspectives to mechanisms. Folia Neuropathol 60: 384-389, 2022.
7. Li M, Tang H, Li Z and Tang W: Emerging treatment strategies for cerebral ischemia-reperfusion injury. Neuroscience 507: 112-124, 2022.
8. Yu L, Zhang Y, Chen Q, He Y, Zhou H, Wan H and Yang J: Formononetin protects against inflammation associated with cerebral ischemia-reperfusion injury in rats by targeting the JAK2/STAT3 signaling pathway. Biomed Pharmacother 149: 112836, 2022.
9. Li L, Jiang W, Yu B, Liang H, Mao S, Hu X, Feng Y, Xu J and Chu L: Quercetin improves cerebral ischemia/reperfusion injury by promoting microglia/macrophages M2 polarization via regulating PI3K/Akt/NF-κB signaling pathway. Biomed Pharmacother 168: 115653, 2023.
10. Zhang Q, Jia M, Wang Y, Wang Q and Wu J: Cell death mechanisms in cerebral ischemia-reperfusion injury. Neurochem Res 47: 3525-3542, 2022.
11. Shi M, Chen J, Liu T, Dai W, Zhou Z, Chen L and Xie Y: Protective effects of remimazolam on cerebral ischemia/reperfusion injury in rats by inhibiting of NLRP3 inflammasome-dependent pyroptosis. Drug Des Devel Ther 16: 413-423, 2022.
12. Zhu XN, Li J, Qiu GL, Wang L, Lu C, Guo YG, Yang KX, Cai F, Xu T, Yuan TF and Hu J: Propofol exerts anti-anhedonia effects via inhibiting the dopamine transporter. Neuron 111: 1626-1636. e6, 2023.
13. Viderman D, Nabidollayeva F, Bilotta F and Abdildin YG: Comparison of dexmedetomidine and propofol for sedation in awake craniotomy: A meta-analysis. Clin Neurol Neurosurg 226: 107623, 2023.
14. Guan S, Sun L, Wang X, Huang X and Luo T: Propofol inhibits neuroinflammation and metabolic reprogramming in microglia in vitro and in vivo. Front Pharmacol 14: 1161810, 2023.
15. Liu J, Ai P, Sun Y, Yang X, Li C, Liu Y, Xia X and Zheng JC: Propofol inhibits microglial activation via miR-106b/Pi3k/Akt axis. Front Cell Neurosci 15: 768364, 2021.
16. Wang D, Sun H, Hai K, Li N, Gu Y and Ma Z: Propofol alleviates traumatic brain injury through regulating Th17/Treg balance by activation of the AMPK/SIRT1 pathway. Toxicol Mech Methods 35: 644-654, 2025.
17. Sun B, Ou H, Ren F, Guan Y, Huan Y and Cai H: Propofol protects against cerebral ischemia/reperfusion injury by down-regulating long noncoding RNA SNHG14. ACS Chem Neurosci 12: 3002-3014, 2021.
18. Gao YY, Tao T, Wu D, Zhuang Z, Lu Y, Wu LY, Liu GJ, Zhou Y, Zhang DD, Wang H, *et al*: MFG-E8 attenuates inflammation in subarachnoid hemorrhage by driving microglial M2 polarization. Exp Neurol 336: 113532, 2021.
19. Dong X, Zhang Z, Shu X, Zhuang Z, Liu P, Liu R, Xia S, Bao X, Xu Y and Chen Y: MFG-E8 alleviates cognitive impairments induced by chronic cerebral hypoperfusion by phagocytosing myelin debris and promoting remyelination. Neurosci Bull 40: 483-499, 2024.
20. Li D, Lu W, Wang R and Ma Y: MFG-E8 in microglial regulation: A review of basic research in the central nervous system. J Food Sci 90: e70235, 2025.
21. Cai Q, Zhao C, Xu Y, Lin H, Jia B, Huang B, Lin S, Chen D, Jia P, Wang M, *et al*: Qingda granule alleviates cerebral ischemia/reperfusion injury by inhibiting TLR4/NF-κB/NLRP3 signaling in microglia. J Ethnopharmacol 324: 117712, 2024.
22. Ou Z, Zhao M, Xu Y, Wu Y, Qin L, Fang L, Xu H and Chen J: Huangqi Guizhi Wuwu decoction promotes M2 microglia polarization and synaptic plasticity via Sirt1/NF-κB/NLRP3 pathway in MCAO rats. Aging (Albany NY) 15: 10031-10056, 2023.
23. Xue K, Qi M, She T, Jiang Z, Zhang Y, Wang X, Wang G, Xu L, Peng B, Liu J, *et al*: Argon mitigates post-stroke neuroinflammation by regulating M1/M2 polarization and inhibiting NF-κB/NLRP3 inflammasome signaling. J Mol Cell Biol 14: mjac077, 2023.
24. Meimei C, Fei Z, Wen X, Huangwei L, Zhenqiang H, Rongjun Y, Qiang Z, Qiuyang L, Xiaozhen L, Yuan Y, *et al*: Taxus chinensis (Pilg.) Rehder fruit attenuates aging behaviors and neuroinflammation by inhibiting microglia activation via TLR4/NF-κB/NLRP3 pathway. J Ethnopharmacol 337: 118943, 2025.
25. Ashrafizadeh M: Cell death mechanisms in human cancers: Molecular pathways, therapy resistance and therapeutic perspective. J Cancer Biomol Ther 1: 17-40, 2024.
26. Lei P, Li Z, Hua Q, Song P, Gao L, Zhou L and Cai Q: Ursolic acid alleviates neuroinflammation after intracerebral hemorrhage by mediating microglial pyroptosis via the NF-κB/NLRP3/GSDMD pathway. Int J Mol Sci 24: 14771, 2023.
27. Cai X, Li Y, Zheng X, Hu R, Li Y, Xiao L and Wang Z: Propofol suppresses microglial phagocytosis through the downregulation of MFG-E8. J Neuroinflammation 18: 18, 2021.
28. Shi X, Cai X, Di W, Li J, Xu X, Zhang A, Qi W, Zhou Z and Fang Y: MFG-E8 selectively inhibited Aβ-induced microglial M1 polarization via NF-κB and PI3K-Akt pathways. Mol Neurobiol 54: 7777-7788, 2017.
29. Xu X, Gao W, Li L, Hao J, Yang B, Wang T, Li L, Bai X, Li F, Ren H, *et al*: Annexin A1 protects against cerebral ischemia-reperfusion injury by modulating microglia/macrophage polarization via FPR2/ALX-dependent AMPK-mTOR pathway. J Neuroinflammation 18: 119, 2021.
30. Tao W, Zhang X, Ding J, Yu S, Ge P, Han J, Luo X, Cui W and Chen J: The effect of propofol on hypoxia- and TNF-α-mediated BDNF/TrkB pathway dysregulation in primary rat hippocampal neurons. CNS Neurosci Ther 28: 761-774, 2022.
31. Beaulieu J, Costa G, Renaud J, Moitié A, Glémet H, Sergi D and Martinoli MG: The neuroinflammatory and neurotoxic potential of palmitic acid is mitigated by oleic acid in microglial cells and microglial-neuronal co-cultures. Mol Neurobiol 58: 3000-3014, 2021.
32. Xian M, Cai J, Zheng K, Liu Q, Liu Y, Lin H, Liang S and Wang S: Aloe-emodin prevents nerve injury and neuroinflammation caused by ischemic stroke via the PI3K/AKT/mTOR and NF-κB pathway. Food Funct 12: 8056-8067, 2021.
33. Zhao R, Zhao D, Zhu X, Li F, Xiong P, Li S and Liu J: The influence of miR-3149 on the malignancy progression of gastric cancer by negatively regulating CEACAM5. J Cancer Biomol Ther 1: 1-10, 2024.
34. Liu J, Zhang X, Guo J, Zhang Y, Fan J, Liu J, Chen J, Jiang J, Yu B, Zhang K and Zhou B: Ursolic acid ameliorates cerebral ischemia-reperfusion injury by inhibiting NF-κB/NLRP3-mediated microglia pyroptosis and neuroinflammation. Front Pharmacol 16: 1622131, 2025.
35. Kong L, Li W, Chang E, Wang W, Shen N, Xu X, Wang X, Zhang Y, Sun W, Hu W, *et al*: mtDNA-STING axis mediates microglial polarization via IRF3/NF-κB signaling after ischemic stroke. Front Immunol 13: 860977, 2022.
36. Zhang Q, Wang L, Chen B, Zhuo Q, Bao C and Lin L: Propofol inhibits NF-κB activation to ameliorate airway inflammation in ovalbumin (OVA)-induced allergic asthma mice. Int Immunopharmacol 51: 158-164, 2017.
37. Gao YY, Zhang ZH, Zhuang Z, Lu Y, Wu LY, Ye ZN, Zhang XS, Chen CL, Li W and Hang CH: Recombinant milk fat globule-EGF factor-8 reduces apoptosis via integrin β3/FAK/PI3K/AKT signaling pathway in rats after traumatic brain injury. Cell Death Dis 9: 845, 2018.
38. Longa EZ, Weinstein PR, Carlson S and Cummins R: Reversible middle cerebral artery occlusion without craniectomy in rats. Stroke 20: 84-91, 1989.
39. Lu J, Li Z, Zhao Q, Liu D and Mei YA: Neuritin improves the neurological functional recovery after experimental intracerebral hemorrhage in mice. Neurobiol Dis 156: 105407, 2021.
40. Pandarathodiyil AK, Ramanathan A, Garg R, Doss JG, Rahman FBA, Ghani WMN and Vijayan SP: Lactate dehydrogenase: The beacon of hope? J Pharm Bioallied Sci 14 (Suppl 1): S1090-S1092, 2022.

41. Zhang L, Dai X, Li D, Wu J, Gao S, Song F, Liu L, Zhou Y, Liu D and Mei W: MFG-E8 ameliorates nerve injury-induced neuropathic pain by regulating microglial polarization and neuroinflammation via integrin β3/SOCS3/STAT3 pathway in mice. J Neuroimmune Pharmacol 19: 49, 2024.
42. Zhong Y, Gu L, Ye Y, Zhu H, Pu B, Wang J, Li Y, Qiu S, Xiong X and Jian Z: JAK2/STAT3 axis intermediates microglia/macrophage polarization during cerebral ischemia/reperfusion injury. Neuroscience 496: 119-128, 2022.
43. Liao J, Wei M, Wang J, Zeng J, Liu D, Du Q, Ge J and Mei Z: Naotaifang formula attenuates OGD/R-induced inflammation and ferroptosis by regulating microglial M1/M2 polarization through BMP6/SMADs signaling pathway. Biomed Pharmacother 167: 115465, 2023.
44. Chen S, Pan J, Gong Z, Wu M, Zhang X, Chen H, Yang D, Qi S, Peng Y and Shen J: Hypochlorous acid derived from microglial myeloperoxidase could mediate high-mobility group box 1 release from neurons to amplify brain damage in cerebral ischemia-reperfusion injury. J Neuroinflammation 21: 70, 2024.
45. Lan Z, Tan F, He J, Liu J, Lu M, Hu Z, Zhuo Y, Liu J, Tang X, Jiang Z, *et al*: Curcumin-primed olfactory mucosa-derived mesenchymal stem cells mitigate cerebral ischemia/reperfusion injury-induced neuronal PANoptosis by modulating microglial polarization. Phytomedicine 129: 155635, 2024.
46. Gong L, Liang J, Xie L, Zhang Z, Mei Z and Zhang W: Metabolic reprogramming in gliocyte post-cerebral ischemia/reperfusion: From pathophysiology to therapeutic potential. Curr Neuropharmacol 22: 1672-1696, 2024.
47. Gao J, Su G, Liu J, Song J, Chen W, Chai M, Xie X, Wang M, Liu J and Zhang Z: A novel compound ligusticum cycloprolactam alleviates neuroinflammation after ischemic stroke via the FPR1/NLRP3 signaling axis. CNS Neurosci Ther 30: e70158, 2024.
48. Zeng L, Hu S, Zeng L, Chen R, Li H, Yu J and Yang H: Animal models of ischemic stroke with different forms of middle cerebral artery occlusion. Brain Sci 13: 1007, 2023.
49. Luo L, Liu M, Fan Y, Zhang J, Liu L, Li Y, Zhang Q, Xie H, Jiang C, Wu J, *et al*: Intermittent theta-burst stimulation improves motor function by inhibiting neuronal pyroptosis and regulating microglial polarization via TLR4/NFκB/NLRP3 signaling pathway in cerebral ischemic mice. J Neuroinflammation 19: 141, 2022.
50. Xu H, Ma Y, Shao L, Fu Y, Luo B, Xia C and Min X: Pan-cancer analysis of DLAT reveals it as a prognostic biomarker involved in immune infiltration of liver hepatocellular carcinoma. J Cancer 16: 2167-2180, 2025.
51. Ermine CM, Bivard A, Parsons MW and Baron JC: The ischemic penumbra: From concept to reality. Int J Stroke 16: 497-509, 2021.
52. Biagioni F, Mastroiacovo F, Lenzi P, Puglisi-Allegra S, Busceti CL, Ryskalin L, Ferese R, Bucci D, Frati A, Nicoletti F and Fornai F: The autophagy-related organelle autophagoproteasome is suppressed within ischemic penumbra. Int J Mol Sci 22: 10364, 2021.
53. Ji W, Ren Y, Wei X, Ding X, Dong Y and Yuan B: Ischemic stroke protected by ISO-1 inhibition of apoptosis via mitochondrial pathway. Sci Rep 13: 2788, 2023.
54. Yang SH and Liu R: Four decades of ischemic penumbra and its implication for ischemic stroke. Transl Stroke Res 12: 937-945, 2021.
55. Candelario-Jalil E, Dijkhuizen RM and Magnus T: Neuroinflammation, stroke, blood-brain barrier dysfunction, and imaging modalities. Stroke 53: 1473-1486, 2022.
56. Anthony S, Cabantan D, Monsour M and Borlongan CV: Neuroinflammation, stem cells, and stroke. Stroke 53: 1460-1472, 2022.
57. Wang H, Zhang S, Xie L, Zhong Z and Yan F: Neuroinflammation and peripheral immunity: Focus on ischemic stroke. Int Immunopharmacol 120: 110332, 2023.
58. Dmitrieva VG, Povarova OV, Skvortsova VI, Limborska SA, Myasoedov NF and Dergunova LV: Semax and Pro-Gly-Pro activate the transcription of neurotrophins and their receptor genes after cerebral ischemia. Cell Mol Neurobiol 30: 71-79, 2010.
59. Liu K, Li L, Liu Z, Li G, Wu Y, Jiang X, Wang M, Chang Y, Jiang T, Luo J, *et al*: Acute administration of metformin protects against neuronal apoptosis induced by cerebral ischemia-reperfusion injury via regulation of the AMPK/CREB/BDNF pathway. Front Pharmacol 13: 832611, 2022.
60. Guo L, Huang Z, Huang L, Liang J, Wang P, Zhao L and Shi Y: Surface-modified engineered exosomes attenuated cerebral ischemia/reperfusion injury by targeting the delivery of quercetin towards impaired neurons. J Nanobiotechnology 19: 141, 2021.
61. Li D, Rongchun W, Lu W and Ma Y: Exploring the potential of MFG-E8 in neurodegenerative diseases. Crit Rev Food Sci Nutr 65: 5587-5601, 2025.
62. Zhao M, Wu Y, Huang L, Wang J and Zhang A: The umbilical cord blood exosome MFG-E8 alleviates hypoxic-ischemic encephalopathy brain injury in neonatal rats by restoring autophagy flux and inhibiting ferroptosis through GSK3β/β-catenin signaling. Regen Ther 30: 321-332, 2025.
63. Cheyuo C, Jacob A, Wu R, Zhou M, Qi L, Dong W, Ji Y, Chaung WW, Wang H, Nicastro J, *et al*: Recombinant human MFG-E8 attenuates cerebral ischemic injury: Its role in anti-inflammation and anti-apoptosis. Neuropharmacology 62: 890-900, 2012.
64. Han YH, Liu XD, Jin MH, Sun HN and Kwon T: Role of NLRP3 inflammasome-mediated neuronal pyroptosis and neuroinflammation in neurodegenerative diseases. Inflamm Res 72: 1839-1859, 2023.
65. Fu J and Wu H: Structural mechanisms of NLRP3 inflammasome assembly and activation. Annu Rev Immunol 41: 301-316, 2023.
66. Li X, Yao M, Li L, Ma H, Sun Y, Lu X, Jing W and Nie S: Aloe-emodin alleviates cerebral ischemia-reperfusion injury by regulating microglial polarization and pyroptosis through inhibition of NLRP3 inflammasome activation. Phytomedicine 129: 155578, 2024.
67. Ruan H, Li W, Wang J, Chen G, Xia B, Wang Z and Zhang M: Propofol alleviates ventilator-induced lung injury through regulating the Nrf2/NLRP3 signaling pathway. Exp Mol Pathol 114: 104427, 2020.
68. Shen G, Lou C, Li Q, Zhao B, Luo Y, Wu F, Jiao D, Fang M and Geng Y: Edaravone dexborneol alleviates cerebral ischemia-reperfusion injury through NF-κB/NLRP3 signal pathway. Anat Rec (Hoboken) 307: 372-384, 2024.
69. Liu PF, Gao T, Li TZ, Yang YT, Xu YX, Xu ZP and Mi WD: Repeated propofol exposure-induced neuronal damage and cognitive impairment in aged rats by activation of NF-κB pathway and NLRP3 inflammasome. Neurosci Lett 740: 135461, 2021.